Sea-spray aerosol particles generated in the surf zone.

A. M. J. van Eijk, J. T. Kusmierczyk-Michulec, M.J. Francius, Gilles Tedeschi, Jacques Piazzola, D.L. Merritt, J.D. Fontana

Sea-spray aerosol particles generated in the surf zone

A. M. J. van Eijk,[1,2] J. T. Kusmierczyk-Michulec,[1,3] M. J. Francius,[4] G. Tedeschi,[4] J. Piazzola,[4] D. L. Merritt,[5] and J. D. Fontana[5]

Received 7 January 2011; revised 11 May 2011; accepted 15 July 2011; published 15 October 2011.

[1] To assess the properties of aerosol particles generated over the surf zone, two experiments were held at the pier of Scripps Institution of Oceanography (SIO), La Jolla CA, and at the pier of the U.S. Army Corps of Engineers Field Research Facility (FRF) in Duck NC. On both sites concentrations of surf-generated sea spray particles, wave parameters and meteorological conditions were measured. The surf-aerosol concentrations in the diameter range 0.2–10 microns were obtained from the difference in aerosol size distributions measured upwind and downwind of the surf zone. It was found that the flux of surf-generated particles at diameters at formation can be expressed in terms of wave energy dissipation, which itself is related to the properties of the incoming wavefield and the bathymetry of the beach. Although the flux can also be modeled in terms of wind speed, this relation is considered to be not universal and limited to low- to medium wind speeds. In Duck NC, two transport experiments were performed under offshore flow conditions. In this case, the surf-aerosol concentrations were obtained from the differences in three aerosol size distributions, measured just before and just behind the surf zone and up to 16 km downwind (out to sea). No significant decrease in concentration was observed at the farthest range, which suggests that an appreciable amount of surf-generated aerosols is advected over tens of kilometers.

Citation: van Eijk, A. M. J., J. T. Kusmierczyk-Michulec, M. J. Francius, G. Tedeschi, J. Piazzola, D. L. Merritt, and J. D. Fontana (2011), Sea-spray aerosol particles generated in the surf zone, *J. Geophys. Res.*, *116*, D19210, doi:10.1029/2011JD015602.

1. Introduction

[2] Aerosols play a fundamental role in physical and chemical processes affecting regional and global climate. The aerosol scattering and absorbing properties determine their interaction with the incoming solar radiation and thus their effect on climate. Absorption reinforces the effect of greenhouse gases on global warming; scattering reduces the radiation reaching the Earth's surface and thus causes cooling [*Jaenicke*, 1984; *Charlson et al.*, 1992; *Andreae*, 1995]. The Intergovernmental Panel on Climate Change concluded that the role of aerosols introduces a larger uncertainty in climate assessment than the radiative forcing attributed to greenhouse gases [*Intergovernmental Panel on Climate Change* (*IPCC*), 2008]. This is due to the heterogeneous spatial and temporal distribution of aerosol particles in the troposphere, their different origins (natural, anthropogenic), and their physical and chemical behavior in the free troposphere, all of which makes it difficult to get an accurate estimation of their climatic impact at regional or global scale.

[3] With 70% of the Earth's surface covered by oceans, sea-salt aerosols formed by the interaction of air and water represent a major component of the natural aerosol mass. They are of fundamental importance in air-sea interaction, and play a dominant role in many aspects of atmospheric chemistry, atmospheric radiation, meteorology, cloud physics and climate [*Laskin et al.*, 2003; *Mallet et al.*, 2003; *Lewis and Schwartz*, 2004; *Mulcahy et al.*, 2008; *Piazzola et al.*, 2009a]. In coastal areas, the aerosols of marine origin become mixed with aerosols originating over land, from natural sources (e.g., dust) as well as from anthropogenic sources such as urban and industrial activities [*Piazzola and Blot*, 2010]. This leads to a very heterogeneous spatial and temporal distribution, which makes the coastal zone especially challenging to model [*van Eijk and de Leeuw*, 1992; *Vignati et al.*, 1998].

[4] The generation of sea-spray aerosols has extensively been studied in the past decades. Two major mechanisms have been identified: bubble-mediated production of jet and film droplets from breaking waves [see, e.g., *Blanchard*, 1963; *Spiel*, 1994, 1997] effective at wind speeds from 4 m/s and up, and production of spume droplets torn directly from wave crests by strong turbulence [see, e.g., *Monahan et al.*, 1986] effective at wind speeds in excess of 10–12 m/s. Additional sea-spray production mechanisms include rain-mediated production [see, e.g., *Blanchard and Woodcock*, 1957] and effervescence of bubbles in gaseous supersaturated waters

[1]TNO, The Hague, Netherlands.
[2]Laboratoire de Mécanique de Fluides, UMR 6598 CNRS, Ecole Centrale de Nantes, Nantes, France.
[3]Institute of Oceanology, Polish Academy of Sciences, Sopot, Poland.
[4]Laboratoire de Sondages Electromagnétiques de l'Environnement Terrestre, UMR 6017 CNRS, Université du Sud Toulon-Var, La Valette du Var, France.
[5]JDF&A Inc., Ramona, California, USA.

0148-0227/11/2011JD015602

[see, e.g., *Stramska et al.*, 1990]. This latter process occurs more prominently in warm, nutrient-rich coastal and shallow waters, where phytoplankton activity may lead to significant oxygen levels in the water and an enhanced production of small bubbles [*Marks*, 2008]. The coastal waters are also more likely to contain suspended matter (anthropogenic pollution, river run-off) that can be scavenged by the bubbles, leading to "dirty" bubbles with modified rise speed and overall bubble kinetics [*Woolf*, 1997]. In turn, this may have a non-negligible impact on sea-spray generation, considering that about 50% of kinetic wave energy is dissipated to generate bubbles [*Terray et al.*, 1996]. These are just a few examples underlining the complexity of the bubble-mediated production mechanism, and demonstrate that there is a need for continued interest in this subject.

[5] As breaking waves are especially abundant in the surf zone, *Monahan* [1995] hypothesized that many more sea-spray aerosols per unit area and time would be generated over the surf zone than at Open Ocean. Indeed, early measurements involving an application of atmospheric electric techniques for the measurement of the electric charge on bubble-produced jet drops had revealed a definite flux of electric charge flowing from the surf zone into the air [*Blanchard*, 1966; *Gathman and Hoppel*, 1970; *Gathman*, 1983]. *Exton et al.* [1985] were the first to recognize the importance of surf aerosol production when making beach aerosol measurement. Lidar observations of the surf zone near Scripps Institution of Oceanography (SIO), La Jolla CA, during the EOPACE (Electro-Optical Propagation Assessment in Coastal Environment) campaign [*Jensen et al.*, 1997] confirmed that ocean waves breaking on a beach created plumes of aerosols with concentrations reaching several orders of magnitude higher than the ambient background levels. The plumes extended 20–30 m above the surf zone and were carried along with the wind [*Hooper and Martin*, 1999].

[6] The quantitative assessment of sea-spray aerosol generation over the surf zone requires a source function, i.e., the number of particles of specific radius produced at the sea surface per unit area and time. While source functions for the surf zone are sparse (see below), much effort has been devoted to the establishment of source functions at Open Ocean. Most source functions have been determined on the basis of experimental observations [see, e.g., *Andreas*, 1998, 2002; *Lewis and Schwartz*, 2004; *O'Dowd and de Leeuw*, 2007] and wind speed is generally used to parameterize the aerosol production in terms of environmental conditions. This suggests that there is a strong correlation between aerosol production, wave breaking and wind speed. While this may be effectively true in deep waters for well-developed wind-generated wavefields, wave breaking is a complex process that may not always be clearly related to the prevailing winds. Therefore, several of the more recent aerosol source functions are expressed in terms of whitecap coverage, i.e., the fraction of white water, which is a more direct measure of the amount of wave-breaking (e.g., *Piazzola and Despiau* [2002], *Clarke et al.* [2006], *Shi et al.* [2009] and *Piazzola et al.* [2009a], building on pioneering efforts by *Monahan et al.* [1986]). However, the vast majority of aerosol source functions are still based on wind speed.

[7] From a hydro-dynamical point of view, the problem of wave breaking on wave propagation onto a beach has extensively been studied. *Thornton and Guza* [1986] proposed a parametric model based on the energy budget method. The model expresses the budget between the energy flux of the incident waves and the dissipation terms, i.e., wave breaking and bottom friction. Neglecting bottom friction and using additional closure models [*Battjes and Janssen*, 1978; *Baldock et al.*, 1998; *Thornton and Guza*, 1986], *Francius et al.* [2007] expressed the local wave-energy dissipation *WED* (associated with wave-breaking) in terms of the bathymetry profile and the characteristics of the incident wavefield. Thus, from a hydro-dynamical point of view, coastal wave-breaking and thereby surf zone sea-spray aerosol generation is related to *WED* rather than wind speed (assuming that spray production is dominated by jet droplet production).

[8] Adopting the hydro-dynamical point of view, *Chomka and Petelski* [1997] suggested that the total aerosol flux in the surf zone is a function of wave energy dissipation. Using dimensional analysis and measurements of the total aerosol flux from two experiments in the Baltic Sea [see also *Petelski and Chomka*, 1996], *Petelski and Chomka* [2000] formulated an expression relating the total aerosol flux to wave energy dissipation (*WED*) to the 3/4 power. They considered this to be a universal relation, applicable to any shoreline where waves are breaking. Coefficients in the equation were different, however, for one set of experimental measurements versus the other.

[9] *Gathman and Smith* [1997] reported aerosol concentrations over the surf zone, measured using a boat (upwind of the surf zone) and a shore-based station (downwind of the surf zone) in San Diego Bay, during one of the 1996 trials of the EOPACE campaign. They observed a concentration increase of 1 order of magnitude and they found a relation between swell height and the concentration of surf aerosol (as inferred from the extinction at electro-optical wavelengths). Since swell height and wave energy dissipation are related, this result supports the hypothesis that wave energy dissipation at the beach is a governing factor for surf aerosol production.

[10] *de Leeuw et al.* [1997] measured aerosol concentrations over the surf zone in onshore winds at La Jolla, CA, during two other trials of the EOPACE campaign in 1996 and 1997. Although they observed concentration increases up to two orders of magnitude for particle diameters from 1 to 10 μm and clear vertical gradients, they could find no clear relation between surf aerosol production and wind speed or wave properties. *Neele et al.* [1998] reported a second look, in more depth, at the results of the EOPACE experiments which now also included data from a pier in Moss Landing, near Monterey, CA. For these data sets, *Neele et al.* [1998] could confirm the 3/4 power relationship proposed by *Chomka and Petelski* [1997]. *de Leeuw et al.* [2000] revisited the EOPACE surf data sets and prior analyses and stated that the 3/4 power relationship worked for part of their data sets, but not for other parts. They then turned away from wave energy dissipation and proposed a simple power law surf source function by correlating measured aerosol number fluxes for various particle diameters at the moment of formation against four different wind speed ranges. Increased aerosol concentrations over the surf zone were later also reported by *Zielinski* [2003], as inferred from lidar observations at various coastal sites of the Southern Baltic Sea. *Zielinski* [2003] also presents a relation between aerosol concentration and wind speed, but he did not study possible relations with other meteorological and/or hydro-dynamical parameters.

[11] *Clarke et al.* [2006] report on a series of observations from a tower at the beach of Oahu, Hawaii. Their in situ aerosol measurements extend down to particle sizes much lower than those achieved in the earlier efforts reported above. The analysis culminates in a universal function for the surface flux of aerosols for a whitecap coverage of 100%, i.e., a function that is not dependent on any environmental parameter. They assume that this universal function scales with the whitecap coverage. This implies that the surf source function (or for that matter, the Open Ocean source function) can be retrieved by multiplying with the whitecap ratio, which is taken to be a function of wind speed following *Monahan et al.* [1986]. This same hypothesis is adopted by *O'Dowd and de Leeuw* [2007] for the surf source function derived by *de Leeuw et al.* [2000], albeit with the difference that *O'Dowd and de Leeuw* [2007] assume a whitecap ratio of 100% over the surf zone.

[12] While the surf source function provides information on the local aerosol concentration, this function needs to be coupled with a transport function to allow assessment of surf aerosol effects at some distance away from the surf zone. The literature is even sparser on transport issues than on surf production, and the few papers available provide contradicting information. As for vertical transport, lidar observations over the surf zone at Scripps Pier CA revealed the presence of surf-aerosol plumes that extended up to 20 m [*Hooper and Martin*, 1999]. Simultaneous in situ aerosol measurements at different heights allowed *de Leeuw et al.* [1997] to infer a gradient function yielding a similar plume height. On the contrary, *Clarke et al.* [2006] present data obtained at Hawaii suggesting that the surf-generated aerosol plumes remain much closer to the surface. They suggest a concentration decrease by one order of magnitude over the first 5 m of altitude. Their results are also confirmed by lidar [*Porter et al.*, 2003] and corroborate with other reports in literature [*Exton et al.*, 1985; *Sievering et al.*, 2004].

[13] Ambiguity also applies to horizontal transport of surf-generated aerosols. For onshore flow, *Petelski and Chomka* [2000] reported a strong decrease in sea salt mass concentration as a function of distance from the shoreline. No salt particles greater than 10 microns were found farther inland than 82 m from the shoreline. In contrast, *Kunz et al.* [2002] concluded from lidar observations on the Irish West Coast that surf-generated aerosols may be transported over distances of several kilometers. *Vignati et al.* [1998, 2001] developed the numerical Coastal Aerosol Transport (CAT) model to assess horizontal transport of surf aerosols in offshore flow. As a first step, *Vignati et al.* [2001] reported encouraging agreement of CAT with nearshore aerosol concentrations measured at the island of South Uist [*Smith et al.*, 1993] and Duck, NC [*Hooper and Martin*, 1999]. The CAT model was then used to predict (surf) aerosol concentrations beyond the surf zone. By initializing the model with data obtained during the EOPACE experiments in California in 1996–97, *de Leeuw et al.* [2000] and *Vignati et al.* [2001] predicted that the effect of the surf zone extended up to several tens of kilometers from the shoreline, both for low and high surf production. Unfortunately, the EOPACE data set did not allow for an experimental verification of these model results.

[14] The above literature survey reveals that there is still uncertainty over the proper environmental parameters to describe the production of surf-generated sea-spray aerosols, as well as their subsequent transport away from the production zone. This provided the impetus for the present paper. We report on two experiments over the surf zone, one at the pier of Scripps Institution of Oceanography (SIO), La Jolla CA, the other at the pier of the U.S. Army Corps of Engineers Field Research Facility (FRF) in Duck NC. On both sites we measured concentrations of surf-generated sea spray particles, wave parameters and meteorological conditions. The surf-aerosol concentrations in the diameter range 0.2–10 microns were obtained from the difference in aerosol size distributions measured upwind and downwind of the surf zone. In Duck NC, we also performed a transport experiment under offshore flow conditions. In this case, the surf-aerosol concentrations were obtained from the differences in three aerosol size distributions, measured just before and just behind the surf zone and up to 16 km downwind (out to sea). In addition, we applied a numerical transport model (MACMod) [*Blot*, 2009; *Tedeschi and Piazzola*, 2011] to obtain numerical simulations of the aerosol concentrations in offshore flow.

[15] Section 2 presents the sites, the experimental set-ups and the procedure to inter-compare the aerosol probes. This procedure is instrumental for obtaining the difference concentrations mentioned above. Section 3 presents the methodologies, and in particular a critical discussion of the model used to convert aerosol concentrations into (mass) fluxes. Results are described in section 4, starting with the spectra of aerosol concentrations, then the spectra of aerosol fluxes, and finally the integrated aerosol mass flux. This section also presents the vertical and larger-scale horizontal variations in the aerosol concentration. Finally, section 5 summarizes the main findings. Although the present paper provides a full discussion of the experiments and subsequent data analysis, technical details are discussed more extensively in two reports by *van Eijk et al.* [2009] and *Piazzola et al.* [2009b].

2. Experimental Setup

2.1. In Situ Aerosol Measurements

[16] The core assets for the experiments consisted of 6 optical particle counters, manufactured by Particle Measuring Systems (PMS), and 1 aerodynamic particle sizer (APS) manufactured by Trust, Science, Innovation (TSI). Table 1 shows the main characteristics of the 7 probes that were deployed. The data of all individual probes was synchronized in time. Probe data was collected in 1-s intervals, and accumulated over 1 min before storing on hard disk. Later, the raw data was reduced by averaging over 5 or 10 min. The software was able to merge data from 2 or more individual probes into a single composite size distribution. This merge process consisted solely of creating a "joint" data-array and did not include any adjustment of individual bin concentrations. The capability to merge data of individual probes allowed for the creation of data files containing size distributions over a wide diameter range from two probes placed side by side. These pairs of probes will be referred to as probe 23, 46, 57 and 78. Thus, the pair of probes 23 yields a size distribution between (nominally) 0.21 and 45.5 μm (see Table 1).

[17] The individual data points in each data file were fitted to a polynomial function in log (*dNdD*) versus log (*D*) space to obtain an analytical function for the aerosol size distribution. This polynomial function is only defined between the smallest and largest diameter in the data file, i.e., no extrapolation was allowed at any time. Since the reliability of the PMS probes becomes significantly less for diameters above

Table 1. Probe Characteristics and Deployment

Identification Number	Type	Size Range Radius (μm)	Number of Channels	Deployed at Scripps	Deployed at FRF
2	PMS CSASP-200	0.21–18.5	31	Yes	Yes
3	PMS CSAP-100HV	0.75–45.5	60	Yes	Yes
4	PMS CSASP-200	0.21–18.5	31	Yes	Yes
5	PMS PCASP-X	0.11–9.0	31	No	Yes
6	PMS CSASP-100HV-ER	1.50–92.0	60	Yes	Yes
7	PMS FM-100	1.50–49.0	20	No	Yes
8	TSI APS 3321	0.49–20.5	53	No	Yes

10 microns due to inlet losses that were not corrected for in the experiments, data for these particle sizes should be not be used in quantitative analyses. This was accomplished by limiting the polynomial fit to an upper diameter limit. This limit was determined for each individual data file and defined as the first bin containing 5 or less counts. In practice, this yields upper diameter limits of approximately 8–15 microns.

[18] All probes had been size-calibrated prior to the experiment by introducing particles of known uniform sizes into the scattering chamber. Unfortunately, an absolute calibration for the number of particles counted per sampled air volume was not possible. As shown by *Reid et al.* [2006], optical particle counters may widely differ in the absolute amount of particles registered. Therefore, all probes were run side by side for 24 to 72h prior and after the experiments. Based on this inter-comparison, correction tables were constructed for the raw data (bin counts) of each individual probe. By combining two correction tables, the correction table for a probe pair was constructed. These correction tables were then used to adjust individual probe and probe-pair responses to a common average size distribution, to which new polynomials were fitted [*de Leeuw et al.*, 2000]. Differences between correction tables before and after the experiment showed that the characteristics of individual probes had changed somewhat over the course of the experiment (e.g., due to decreasing laser power, contamination of optics). It was assumed that these changes had taken place gradually, and the final correction tables were constructed on the basis of all inter-comparison data (both before and after the experiment). Although the inter-comparison reveals the systematic differences between the concentrations as measured by the various probes, the analysis does not permit selecting a probe (combination) that provides the best measurements in an absolute sense. For this, an additional measurement (e.g., the total aerosol mass as provided by a filter method) is required, which is not available. The absence of an absolute gauge for the aerosol concentration implies that our measurements allow for the determination of functional dependencies between aerosol concentration and for example, wave energy dissipation, but that there is a remaining uncertainty in the values of constants.

[19] The inter-comparisons were crucial to the experiments, since the concentrations of surf-generated aerosols were assessed from concentration differences as measured upwind and downwind of the surf zone. After correction to the common average size distribution, the average residual difference concentrations $\langle \Delta_{A\text{-}B}(D) \rangle$ were determined for each combination of probes A and B:

$$\langle \Delta_{A-B}(D) \rangle = \frac{1}{M} \sum_{i=1}^{M} \left({}^{10}\log\,(dN/dD)_A - {}^{10}\log\,(dN/dD)_B \right) \quad (1)$$

where the index i runs over all M pairs of individual aerosol data files, and dN/dD is calculated from the polynomial fits to the corrected data. This allows evaluating dN/dD at arbitrary diameter, instead of being restricted to the center diameters of the bins. The values of $\langle \Delta_{A\text{-}B}(D) \rangle$ provide a measure for the success of the inter-comparison: smaller values suggest that the (corrected) size distributions of two probes A and B are relatively close. Consequently, the values of $\langle \Delta_{A\text{-}B}(D) \rangle$ provide an indication for the minimum resolvable concentration difference between probe combination A and B. Because the individual values of $\Delta_{A\text{-}B}(D)$ for two simultaneously measured aerosol records can be larger than $\langle \Delta_{A\text{-}B}(D) \rangle$, we consider $\langle \Delta_{A\text{-}B}(D) \rangle$ an optimistic estimate of the minimum resolvable concentration difference. Figure 1 (top) shows spectra of $\langle \Delta_{A\text{-}B}(D) \rangle$ for three pairs of probes. The curve with circles, for probe combination 46–23, applies to the inter-comparison for the FRF experiment, but inter-comparison results for the Scripps experiment were comparable. The other curves apply to probe combinations only used at FRF (see Table 1). Figure 1 (bottom) shows that the standard deviations in the values of $\langle \Delta_{A\text{-}B}(D) \rangle$ are generally below 0.3 log unit (a factor of 2). We will take this value as the minimum resolvable concentration difference for our probe combinations. Figure 1 shows that the difference concentra-

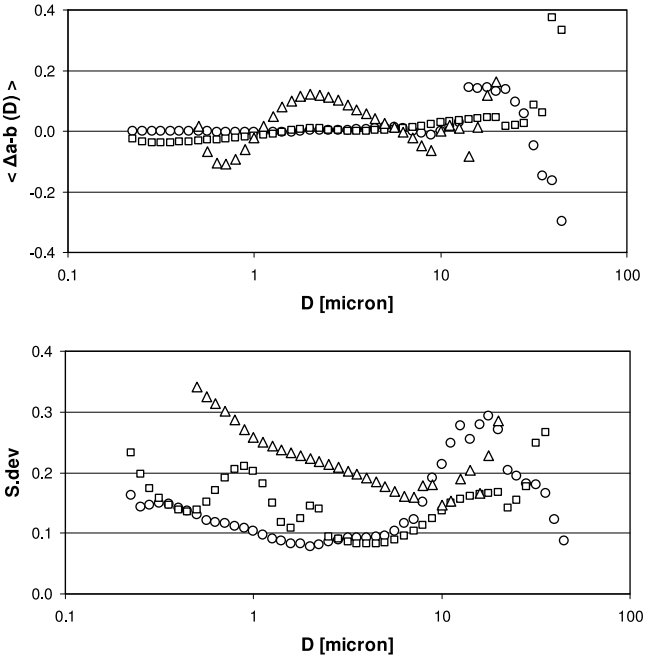

Figure 1. Inter-comparison results for probes 46–23 (circles), 46–78 (triangles) and 46–57 (squares).(top) Residual $\langle \Delta_{A\text{-}B}(D) \rangle$ factors. (bottom) Standard deviations in $\langle \Delta_{A\text{-}B}(D) \rangle$.

Table 2. Ranges of Environmental Parameters Encountered During the Experiments

Parameter	Unit	Scripps		FRF	
		Min - Max	Average	Min - Max	Average
Wind speed	ms^{-1}	0–8	1	0–21	4
Relative humidity	%	40–100	90	40–100	82
Air temperature	°C	10–25	16	7–28	22
Wave height	m	0.3–2.2	0.8	0.5–4.5	0.6
Wave period	s	3–15	9	5–15	9
Wave energy dissipation	Wm^{-2}	10–70	22	10–180	26

tions are relatively more reliable in the domain below 10 μm. The scatter in $\langle \Delta_{A\text{-}B}(D) \rangle$ and the increased standard deviations at larger diameters suggests that the effective upper limit of the aerosol spectra measured in the experiment was of the order of 10 microns.

2.2. Aerosol Measurements on a Larger Spatial Scale

[20] Information about the aerosols in the Scripps area was acquired with the TNO 7-wavelength transmissometer, operating in 7 bands between 0.4 and 13.7 μm. A 6.7 km transmission link was set up between the end (ocean-side) of Scripps pier and the entrance to Torrey Pines State Park. The transmissometer provided the path-averaged extinction for the 7 wavelength bands. After removing the molecular contribution from the signals, an iterative procedure was used to estimate the aerosol size distribution from the aerosol extinctions, using Mie-theory. Further details about the instrument, the experimental set-up and the determination of the aerosol size distribution are given by *de Jong et al.* [2007] and *Kusmierczyk-Michulec et al.* [2008].

[21] Two Sun photometers were operated at Scripps. One photometer was a MICROTOPS II, mounted on a tripod and provided by SPAWAR Systems Center (SSC) Pacific, San Diego; the other an automated CIMEL Sun photometer, part of the AERONET network, which was temporarily relocated to Scripps pier. At Duck, the handheld MICROTOPS II Sun photometer was deployed. The Sun photometers measured the optical depth from ground to the top of the atmosphere in the direction of the sun, at 5–7 wavelengths between 0.34 and 1.02 μm. The data were analyzed with AERONET standard procedures to retrieve aerosol optical depth, Ångström coefficient and size information [*Holben et al.*, 2001; *Dubovik and King*, 2000; *Smirnov et al.*, 2000]. Only quality-assured and cloud-free data (level 2) data were used.

[22] Aerosol properties on a synoptic scale were assessed from air mass backward trajectory analysis, which trace the history (location and height) of an air mass back in time from the location of interest. For Scripps, 7-day backward trajectories were available from AERONET, and their calculation is based on the National Aeronautics and Space Administration (NASA) Goddard kinematic trajectory model [*Schoeberl and Newman*, 1995; *Pickering et al.*, 2001]. At Duck, 4-day backward trajectories were calculated using the public-domain NOAA ARL HYSPLIT (HYbrid Single Particle Lagrangian Integrated Trajectory) model (http://www.arl.noaa.gov/).

2.3. Wave and Meteorological Data

[23] At Scripps, the wavefield data were obtained from three different sensors: 1) a CDIP (The Coastal Data Information Program) buoy operated by the Ocean Engineering Research Group at SIO; 2) a SIO pressure sensor mounted on the second piling from the north, on the west end of the pier, 15.13 m below the top surface of the pier deck; and 3) an Acoustic Doppler Velocimeter (ADV) operated by the Southern University of Toulon-Var, lowered into the water adjacent to the southwest end of the pier, about 10 m from the end of the pier. At Duck, wavefield data were obtained from the FRF Sensometric SP793(C) array of 15 pressure-gauges (ID 3111), located at 8 m depth at 1 km offshore from the pier. Tide information was obtained from the NOAA Tide station (ID 8651371), located at the end (ocean-side) of the pier. At both sites, the Southern University of Toulon-Var operated a high-resolution video camera to make recordings of the surf zone. These recordings were analyzed with image processing techniques to estimate the length of the surf zone.

[24] Bathymetry profiles were required for the calculation of wave energy dissipation (WED). Bathymetry measurements around Scripps pier were made one week prior to the start of the experiment by a contractor, Applied Technology and Research, Encinitas CA. The bathymetry profile resembled closely a plane beach with constant slope equal to 1/3 and isobaths parallel with the alongshore direction. At FRF, the bathymetry was surveyed by the FRF staff on October 11th. The bathymetry profile at FRF was more irregular than at Scripps, and two transects, north and south of the pier, were used for the calculations. The resulting values of wave energy dissipation did not differ significantly. The local bathymetry was surveyed again on November 6th after the passing of tropical storm Noel, and it was found that it had not significantly changed due to the passing of Noel.

[25] Meteorological data was recorded by the standard instruments deployed by SIO and FRF on their piers. In both experiments, the TNO meteorological station made additional recordings of wind speed, wind direction, relative humidity, air and sea temperatures and rainfall at location near the end (ocean-side) of the piers. All data was reduced to 5 min averages and stored with the aerosol data. Table 2 lists the ranges of relevant environmental parameters as encountered during the two experiments. Table 2 shows an important difference between the two sites: at FRF, both the peak values and the average values of wind speed and wave energy dissipation were much higher than at Scripps. The larger dynamic ranges of these two key parameters are paramount to the analysis presented below. The Scripps experiment was characterized by exceptionally fair weather with pleasant temperatures and low winds. The site was subject to a very regular sea-breeze, resulting in onshore winds during the day and offshore winds during the night. In contrast, the weather at FRF was far more irregular and more extreme. The passing of a tropical storm caused strong winds and high waves, and these high waves lasted for several days after the passage of the storm. Because onshore and offshore flow conditions pertained for several days, the final data set for FRF consists of a limited number of longer onshore and offshore "flow events" (3 each) as opposed to Scripps.

2.4. First Experimental Site: Scripps Pier

[26] The first experiment took place from 2 to 29 November 2006 at the pier of Scripps Institution of Oceanography (SIO) in La Jolla, California. The Scripps pier is 330 m long, starting from the back of beach and projecting well beyond the surf zone even at low tide. The deck of the pier is 10.25 m

Figure 2. (top) SIS at FRF pier. (bottom) Wahoo with aerosol probes 23 (white boxes).

above mean low water level and the pier is oriented toward the west northwest, 288° from true north. Behind SIO, the coastal hills rise quickly to a height of about 125 m. This may impact on the larger-scale airflow patterns in that area.

[27] In deciding where to place the PMS probes, locations were sought that would provide undisturbed airflow into the probe as much as possible. At the outer end of the pier, the probe pair 23 was placed at approximately 13 m above the ocean on top of one of the storage buildings, right at the outer edge of the building and facing the ocean. This ensured the best measurement conditions during onshore winds. For offshore winds, however, sampling may have been less optimal. First, the inlet horns were not turned into the offshore winds, but remained ocean-facing. While prior experience had shown that in low wind speeds (a few m/s) the forced convection produced by the probe's internal fan provides enough suction to draw in adequate samples, some under-sampling cannot be ruled out. This is especially true for the larger diameters as no correction was made for inlet losses. Furthermore, in offshore flow the deck of the pier becomes a possible source of obstruction for the aerosols generated at the sea surface, which can again cause under-sampling. However, since the wind direction was rarely exactly aligned with the pier, aerosol plumes generated left or right of the pier should have been able to reach the probe's location.

[28] On the shore end, selecting a location for the PMS probes was more difficult. *de Leeuw et al.* [1997] had placed their probes immediately next to the pier (south side), but the analysis by *Neele et al.* [1998] suggested that the sun-heated pier deck had affected the measurements. To avoid adverse effects by the pier, a location 168 m south of the pier was chosen for the present experiment. In view of the relatively uniform bathymetry along the beach, it was assumed that the surf-aerosol production would be relatively homogeneous along the beach, which means that a (modest) shift in probe location over the alongshore coordinate does not change the experiment. The onshore site was a lawn with no immediate buildings behind the probes. The probe pair 46 was set facing the ocean, at the edge of a short steep slope coming up from the sea wall at the back of the beach. The height of probes was about 9.5 m above the mean water level. For onshore winds, these probes had an unobstructed view of the ocean. Consistent with the probes at the end of the pier, the inlet horns were not turned around in offshore flow.

2.5. Second Experimental Site: FRF Pier

[29] The second experiment took place from 16 October–9 November 2007 in Duck NC at the pier of the Field Research Facility (FRF) of the U.S. Army Corps of Engineers. The pier is 560 m long, extending well beyond the surf zone. The deck of the pier stands 7.7 m above mean low water level and the pier is oriented 75° from true north. The pier is located on a 650 m wide strip of land, separated by Currituck Sound from the U.S. mainland. Contrary to Scripps, the flat land and body of water ensure an unobstructed airflow.

[30] The FRF pier is equipped with the Sensor Insertion System (SIS), shown in the top panel of Figure 2. The SIS is a crane-like device with two arms that reach 15–25 m out from the side of the pier. The two arms can be raised or lowered independently, and rotated 360° around a base mounted on a railroad car that rides on rails running the full length of the pier. The SIS offered a flexible platform for positioning the aerosol probes upwind or downwind of the surf zone while avoiding interference from the pier structure. By rotating the SIS arms from one side of the pier to the other, the probes could be kept on the upwind side of the pier when the wind direction was at an angle to the pier axis, thus avoiding having the probes sit in the wake of the pier.

[31] Figure 3 shows the probe configurations during onshore and offshore flow. The two arms of the SIS were at approximately 6 and 16 m above the water level. Apart from the SIS, two more locations were chosen for aerosol measurements. The top of a container at the end (ocean-side) of the pier provided a location to measure the background concentration during onshore flow at about 10 m above the low water line. A table next to the FRF building (behind the pier) provided a location to measure the background concentration during offshore flow, at about 1.2 m above the ground and at approximately 9 m above the low water line. This location was not ideal, but provided the best compromise between available locations and exposure to the dominant wind directions during offshore flow. Probes 5 and 8 were permanently located at the ocean and land sites, respectively. Probe 7 was moved back and forth between the table and the container to extend the size distribution to larger particles during offshore and onshore flow, respectively. Toward the end of the experiment, probe 5 broke down and probe 8 was then also moved back and forth, along with probe 7.

[32] In view of the larger wind speeds encountered at FRF as compared to Scripps, the inlet horns of all aerosol probes were

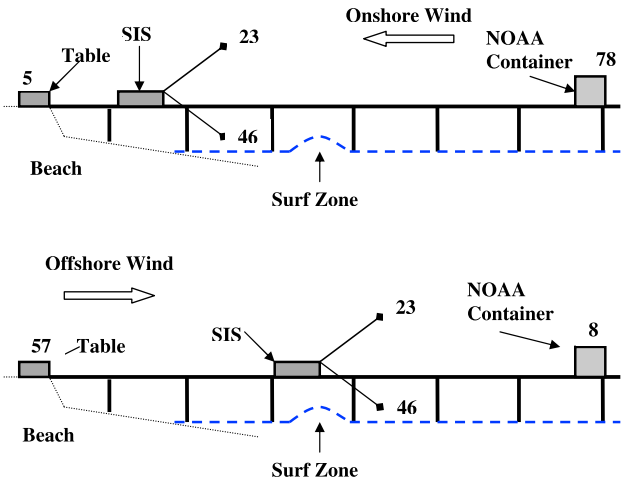

Figure 3. Aerosol probe locations during the FRF experiment. Numbers refer to probes (see Table 1).

always pointed into the wind to avoid under-sampling. As at Scripps, the contribution of surf-generated aerosols was assessed from difference concentrations. For onshore flow, the probe combinations 78 and 46 provided the primary data for these differences, whereas the probe combinations 57 and 46 provided the primary data during offshore flow (see Figure 3). Probe combinations 23 and 46 provided the data for assessing the vertical dispersion of the surf aerosols.

2.6. Transport Experiments at FRF

[33] The transport of surf-generated aerosols was assessed by measuring difference concentrations between the production zone and a distance downwind. For this purpose, a 13 m commercial tuna fishing boat, the Wahoo (Figure 2, bottom) was chartered. For the transport experiment, the aerosol probe pair 23 was relocated from the SIS to the top of the boat's main cabin. In addition, a small portable meteorology station was mounted next to the probes. During steady offshore flow conditions, the Wahoo sailed to the end of the pier for a baseline comparison with probe pair 46, still mounted on the lower arm of the SIS and positioned downwind of the surf zone. Care was taken that the pier did not obstruct the airflow from the surf zone to the Wahoo. Then, the Wahoo traveled along the offshore wind vector to a distance of approximately 15 km before sailing back to the pier for a final comparison. Typically, 10 stops were made during this trip (6–7 on the outbound run and 3–4 on the inbound run) and at each waypoint the aerosol distribution was sampled for approximately 15 min. The whole experiment lasted about 4 h and was performed twice, on 5 and 6 November 2007, during relatively steady offshore flow conditions (constant wind speed and wave height). The data obtained at each waypoint was subsequently averaged into a single data file and corrected to the "average distribution" obtained from the inter-comparisons.

3. Methodology

3.1. Calculation of Wave Energy Dissipation

[34] *Francius et al.* [2007] provide a detailed description of the calculation of wave energy dissipation. They applied a semi-empirical model based on the integration of the wave energy balance equation, which can be written in general form as

$$\frac{d}{dx}\left(EC_g\cos\theta\right) = -\varepsilon_b - \varepsilon_f \tag{2}$$

assuming that linear water wave theory is valid and considering obliquely incident waves on a coastline with straight and parallel contours. In equation (2), x is the cross-shore coordinate and θ is the mean angle of incidence of the wavefield. E is the total wave energy per unit surface area and C_g is the wave group velocity, which are expressed as the general linear wave theory equations for finite depth. Applying finite depth relations implies that reflection of wave energy can be neglected and that the cross shore variations of the bottom profile occur on larger scales than that of the wavefield. The terms on the right hand-side of equation (2), ε_b and ε_f, represent the contributions to the averaged (over time) value of the local dissipation of wave energy due to depth-induced wave breaking effects and bottom friction effects, respectively. These latter effects are commonly small compared to dissipation, and hence, ε_f is neglected.

[35] The dissipation function ε_b is modeled with *Battjes and Janssen*'s [1978] model for a periodic wave bore, which requires a distribution function $p_b(H)$ of breaking wave heights for closure. Since this function is not known, an additional closure model is needed that provides a relation between the breaking waves, the local wave height and the local water depth h. Three of such models by *Battjes and Janssen* [1978], *Thornton and Guza* [1986] and *Baldock et al.* [1998] were tested, and these all yielded similar results when it came to the values of WED. The model by *Baldock et al.* [1998] was retained, because it not only applies to plane, mildly sloped beaches, but also to steep and/or non-planar beaches.

[36] The local water depth h is the sum of the bottom depth below still water level, h_0, and a variation in mean water level of the mean surface, η, that represents wave-driven effects which are associated with shoaling and breaking waves. The variations η are calculated according to *Longuet-Higgins and Stewart* [1963]:

$$\frac{\partial S_{xx}}{\partial x} + \rho g(h_0+\eta)\frac{\partial \eta}{\partial x} = 0 \tag{3}$$

where the radiation stress component, S_{xx}, is calculated according to linear wave theory and h_0 is obtained from the measured bathymetry profile. Numerical integration of equations (2) and (3) from an offshore position to the shoreline then yielded the cross-shore variations of the wave height and the mean wave energy dissipation. The results were validated using benchmark studies reported in literature, for both laboratory and field conditions.

3.2. Calculation of Aerosol Difference Concentrations

[37] As mentioned above, the concentrations of surf-generated aerosols are assessed from differences in the aerosol concentration measured upwind and downwind of the surf zone. To do this, the analytical representations of the size distribution (see section 2.1) are used to evaluate:

$$\delta(D) = (dN/dD)_{down} - (dN/dD)_{up} \tag{4a}$$

$$\delta_{\log}(D) = {}^{10}\mathrm{Log}(dN/dD)_{down} - {}^{10}\mathrm{Log}(dN/dD)_{up} \tag{4b}$$

for 60 diameters ranging between 0.1 and 100 μm. Note that this is a numerical grid; the experimental data does not necessarily cover the full grid. The differences $\delta(D)$ are taken to represent the aerosol size distribution of the aerosols generated over the surf zone, as measured at the height above the sea surface of the downwind probe (a varying parameter due to tidal effects). Since the upwind and downwind probes were generally not positioned at the same height, the latter statement implies that the background aerosols (measured upwind) were well-mixed, i.e., that there was no (significant) vertical gradient in the background concentration. Considering the small difference in probe heights (typically less than 5–10 m), the small gradients observed over the Ocean [cf. *de Leeuw*, 1993], and the relatively small concentration of background aerosols as compared to surf-generated aerosols (see section 4.3), this assumption seems justified.

3.3. Definition of Onshore and Offshore Flow Conditions

[38] The measurement of difference concentrations required that the probes upwind and downwind of the surf zone measured the same air mass, which translated into the requirement of wind directions perpendicular to the beach (or more precisely: along the line between the shore and ocean probe locations). Since a rigorous application of this criterion would yield a very limited amount of aerosol data, intervals of 120° on the wind rose were selected to represent onshore and offshore flow. The center of each interval corresponded with the orientation of the pier. E.g., for the FRF pier at the East Coast, oriented 75° from true North, the terms 'onshore' and 'offshore' in our analysis correspond to two wind direction intervals on the wind rose of 195–315°N and 15–135°N, respectively. In a worst case scenario, this implies that an air mass flowing over the probe positioned at the end of the pier "missed" the other probe station by 300 m on the alongshore axis. In view of the bathymetry measurements, it seems reasonable to assume that the surf production was homogeneous over this distance.

3.4. Model for Evaluating Aerosol Fluxes

[39] In order to obtain the surf aerosol source strength, the concentrations measured at some distance and height from the production zone need to be transformed into the concentration flux at the surface in the production zone. This transformation can be made by applying the continuity (mass conservation) equation:

$$\frac{\partial n_D}{\partial t} + \frac{\partial}{\partial x}(n_D U) + \frac{\partial}{\partial z}\left(\overline{n_D' w'} - n_D V_t\right) = S_{n_D} \tag{5}$$

where n_D is the concentration of aerosols of diameter D at location (x, z), U is the mean horizontal wind speed, V_t is the terminal fall velocity, w' is the fluctuating part of the vertical wind velocity, and n' is the fluctuating part of the concentration field, and S_{nD} is the concentration volumetric gain or loss. If we integrate the equation over a height interval, we obtain:

$$\begin{aligned} j(z_1) - j(z_2) &= f_{eff}(z_1) - f_d(z_1) - j(z_2) \\ &= \int_{z1}^{z2}\left(\frac{\partial n_D}{\partial t}\right) dz + \int_{z1}^{z2}\frac{\partial}{\partial x}(n_D U)\, dz - \int_{z1}^{z2} S_{n_D}\, dz \end{aligned} \tag{6}$$

where j denotes the mean net vertical flux, f_{eff} is the effective production flux and f_d is the deposition flux. Equation (6) is simplified by a number of assumptions: (a) stationary conditions apply ($\partial/\partial t = 0$); (b) U is independent of (x, z) over the surf zone; (c) U has a positive value for onshore flow; (d) there is no volumetric gain or loss between heights z_1 and z_2 ($S_n = 0$); (e) surf-generated particles are contained in the height domain up to z_2 ($j(z_2) = 0$); (f) the x-derivative can be approximated as the difference between the beginning of the surf zone and the shore line divided by the length of the surf zone L; (g) the deposition flux at z_1 is much smaller than the production flux. The latter assumption will break down for those diameters where the production strength is small (very small or very large particles) and for those diameters where the deposition flux is large (very large particles). In practice, this poses severe doubts on the validity of the assumption for diameters larger than (approximately) 10 microns. With these assumptions, we obtain:

$$f_{eff}(z_1) = \frac{U}{L}\left[\left(\int_{z1}^{z2} n_D dz\right)_{shore} - \left(\int_{z1}^{z2} n_D dz\right)_{pier}\right]. \tag{7}$$

[40] To further simplify equation (7), we assume that the aerosols upwind from the surf zone (the "background" concentration on which the surf contribution will be superimposed) are well-mixed with respect to height between z_1 and z_2. This assumption is considered justified in view of the order of magnitude difference in surf and background aerosol concentrations. Finally, the diameter dependence is made explicit to obtain:

$$\left(\frac{dF(D)}{dD}\right)_{surf} = 10^6 \frac{U}{L}\left[\int_0^{z\max}\left(\frac{dN(z,D)}{dD}\right)_{surf} dz\right] \tag{8}$$

where the subscript *surf* denotes the surf contribution (obtained by subtracting the concentrations measured by the probes after the surf zone from those before the surf). The integral now runs from the surface, where we want to evaluate dF/dD, to a height $z_{\max}$ which must at least correspond to the maximum height the surf aerosols can attain. The factor 10^6 is added to express dF/dD in units of [μm^{-1}.m^{-2}.s^{-1}]. The flux dF/dD can be converted into a volume flux dF_v/dD in units of [μm^{-1}.m.s^{-1}] by multiplying with $\pi D^3/6$. The inputs to equation (8) are the dN/dD values at ambient humidity (assuming that the surf-generated droplets adjust rapidly to the ambient humidity [cf. *Andreas*, 1992]), which thus yields the source function dF/dD at ambient humidity. However, it is customary to specify the source function dF/dD either in a standard environment of 80% humidity or for diameters at formation. We have chosen to express dF/dD as diameters at formation, and the conversion of the dF/dD values was made with an iterative algorithm evaluating droplet density at ambient humidity using seawater salinity as input [*van Eijk et al.*, 2001].

[41] The theoretical framework outlined in equations (5)–(8) relates the flux at the surface to the concentration of surf-generated particles at some distance downwind from the production zone. This approach can be visualized by a box, where particles enter the box at the source (vertical flux of surf-generated particles) and leave the box through the vertical

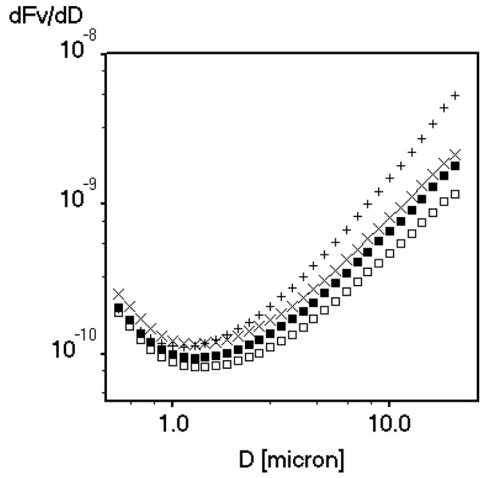

Figure 4. Sensitivity of aerosol volume fluxes dF_v/dD, in $[\mu m^{-1}.m^{-2}.s^{-1}]$ and for onshore flow at Scripps, to flux model parameterizations. Solid squares: default parameterization given by equations (5)–(11); crosses: effect of using L_0 instead of L; open squares: effect of changing z_{ref} by −1 m; pluses: effect of 33% steeper gradient function ζ.

plane at the downwind location of the detector (PMS-probe, horizontal flux out of the box). It is evident that this model requires that all particles are transported from the production zone to the receptor plane. In other words, this model will break down in the absence of wind (or at very low wind speeds) as the deposition flux has been neglected.

3.5. Parameterizations Used for the Flux Model

[42] The evaluation of equation (8) requires explicit expressions for the vertical concentration profile of the surf aerosols and the length of the surf zone. The latter quantity is obtained from the high-resolution video recordings of the surf zones at Scripps and FRF as made by the Southern University of Toulon-Var. Following *Neele et al.* [1998], the surf length L in equation (8) is taken to be an effective surf length, defined as:

$$L = \frac{L_0}{\mid \cos\left(WD - A_{pier}\right) \mid} \tag{9}$$

where WD is the wind direction, A_{pier} is the alignment of the pier along the wind rose, and L_0 is the length of the surf zone taken perpendicular to the beach evaluated from the video recordings. The effective surf length accounts for the longer path of the air mass over the production zone in the case that the wind is not aligned with the pier.

[43] Following *de Leeuw et al.*'s [1997] analysis at Scripps, it is assumed that the height dependence of the surf-generated aerosol concentration in equation (8) is described by an exponential function:

$$\frac{dN(z,D)}{dD} = \frac{dN\left(z_{ref},D\right)}{dD} * \exp\left[\zeta\left(z - z_{ref}\right)\right] \tag{10}$$

where z_{ref} corresponds to the (tide-corrected) height of the PMS probe downwind of the surf zone. The exponential profile corresponds to a balance between production and deposition in the absence of other factors such as advection and the growth of the internal boundary layer. While such conditions are unlikely over the surf zone, the available experimental data did not allow for a more precise determination of the shape of the profile function.

[44] From their measurements at 7 and 15 m height at the base of Scripps pier (50–100 m downwind of the production zone), *de Leeuw et al.* [1997] calculated diameter and wind speed dependent gradient functions ξ. A fit to their Figure 5 yields:

$$\zeta = -0.075 * \frac{(1 + {}^{10}\log D)}{(1 + 0.33\,U)} (U < 9\mathrm{m/s}, 0.2 < D < 40\mu\mathrm{m}) \tag{11}$$

where D is the diameter of the aerosol particle and U is the wind speed. Equation (11) results in larger gradients for larger particles and/or decreasing winds, which is in accordance with experimental data and theoretical considerations. We have made profile measurements at FRF (using the two arms of the SIS), but as will be discussed later, the location of the SIS was such that the plumes may not have fully reached the upper arm. This complicates the evaluation of the gradient functions, and therefore equation (11) has been used for all calculations (at Scripps and at FRF) for the sake of consistency and for inter-comparison of results.

[45] The final parameter that is needed to evaluate equation (8) is z_{max}, the top of the vertical integration domain. In physical terms, z_{max} should be set to at least the maximum height that the surf-aerosol plumes attain, which, as discussed in the introduction, is subject of debate in the literature. However, because equations (10)–(11) fully determine the vertical concentration profile, the numerical requirement for z_{max} is to set it sufficiently large as for the concentration to drop off to negligible contributions to the integral. In practice, a value of 50 m was adequate.

[46] Figure 4 assesses the sensitivity of the flux calculations to the parameterizations discussed above. The Figure displays average volume fluxes dFv/dD in $[\mu m^{-1}.m^{-2}.s^{-1}]$ at diameter of formation as observed during onshore flow conditions at Scripps, but the study could as well have been made with artificial data. The data labeled with solid squares denote the fluxes calculated using the framework defined by equations (5)–(11). Then, the data labeled (x) shows the effect of not correcting for the effective surf length (equation (9)), and the data labeled with open squares shows the effect of estimating the probe heights (z_{ref} in equation (10)) wrong by −1 m. The data labeled with pluses shows the effect of a steeper gradient function, by taking a constant of −0.1 instead of −0.075 in equation (11). In our opinion, the variations in L, z_{ref} and ζ are realistic, i.e., it is reasonable to estimate a probe height wrong by 1 m, and the change in ζ corresponds to the experimental uncertainty in the underlying measurements. Figure 4 shows that the fluxes of larger particles are more sensible to changes in L, z_{ref} and especially ζ. This is unfortunate, since these larger particles represent a significant contribution to the total volume flux and at the same time their concentration gradients are difficult to assess, at least from the data available to the authors.

3.6. Surf-Aerosol Mass Fluxes

[47] The mass flux F_M in [μg.m^{-2}.s^{-1}] of surf-generated aerosols is found by integrating the (volume) fluxes at radius of formation over diameter:

$$F_{M,wet} = \int_{D\min}^{D\max} \left.\frac{dF_V(D)}{dD}\right)_{surf} \rho_{drop}\, dD = \int_{D\min}^{D\max} \left.\frac{dF(D)}{dD}\right)_{surf} \frac{\pi}{6} D^3 \rho_{drop}\, dD \quad (12)$$

$$F_{M,dry} = \int_{D\min}^{D\max} \left.\frac{dF_V(D)}{dD}\right)_{surf} \left(\frac{D_{dry}}{D}\right)^3 \rho_{SS} dD \approx 34.9 \int_{D\min}^{D\max} \left.\frac{dF_V(D)}{dD}\right)_{surf} dD \quad (13)$$

Where $F_{M,wet}$ is the surf-aerosol mass flux and $F_{M,dry}$ is the sea-salt mass flux, ρ_{drop} denotes the density of the aerosols (ρ_{drop} = 1024.7 kg.m^{-3} for a salinity of 34‰), ρ_{SS} denotes the density of sea-salt (ρ_{SS} = 2165 kg.m^{-3}), D is the diameter of the fresh sea spray particle at formation, and D_{dry} the diameter of the dry sea-salt particle. The ratio of D and D_{dry} is constant at 3.96, whereas the ratio of $F_{M,wet}$ and $F_{M,dry}$ is constant at 29.4.

[48] The integration should run over the full size spectrum of the surf-aerosols. In practice, the inability of the aerosol probes to measure particles smaller than 0.1–0.2 μm and the reduced reliability of the PMS-probes at larger diameters limited the spectrum from approximately 0.5 to 20 μm at diameter of formation (roughly 0.25–10 μm aerosol diameter at ambient humidity). Figure 4 suggests that this limited domain will result in an underestimate of the total mass flux F_M by not taking into account the fluxes at smaller and in particular the larger diameters. A numerical test showed that the value of F_M decreased by 10% when changing the lower limit of the integration domain from 1.0 to 0.5 μm, and by a factor of 2 when changing the upper limit of the integration domain from 20 to 15 μm. From these numbers, the shape of the aerosol flux spectrum $dF_v(D)/dD$ (shown in Figure 7; see below), and an extrapolation thereof we estimate, as an order-of-magnitude number, that our calculations may be short of the total mass flux by a factor of 5.

4. Results and Discussion

4.1. Background Aerosols: Scripps

[49] As mentioned in the introduction, the contributions of surf-generated aerosols have been assessed from difference concentrations upwind and downwind of the surf zone. The surf-aerosol concentrations are thus superimposed on a background concentration, advected over the surf zone from sea (onshore flow) or land (offshore flow). Before turning our attention to the surf-aerosols, the properties of these background aerosol concentrations are assessed to characterize the larger-scale environment of the experiments.

[50] For Scripps, the results of the transmissometer and Sun photometer measurements have already been discussed by *de Jong et al.* [2007] and *Kusmierczyk-Michulec et al.* [2008]. Based on air mass backward trajectory analysis, the latter authors demonstrate that the background aerosols at Scripps generally consisted of a mixture from marine and land-based sources. Exceptions occurred during the last days of the experiment (27–28 Nov 2006), when onshore flow brought pure marine air masses to Scripps, and on 7 Nov 2006, when Santa Ana winds caused an (stronger) offshore flow with warm desert air and very low humidity. *Kusmierczyk-Michulec et al.* [2008] confirmed this analysis with a study of the Ångström coefficient, a measure for the spectral variation of the aerosol extinction [*Ångström*, 1929]. As shown by *Kusmierczyk-Michulec and van Eijk* [2007], the value of the Ångström coefficient can be used as a tracer for the ratio of sea spray and land-originated aerosols. Low Ångström coefficients, indicative for pure marine air, were almost exclusively observed on 27–28 Nov.

[51] Background aerosol concentrations at Scripps were assessed by the probes at the end (ocean-side) of the pier during onshore flow (upwind of the surf zone), and by the shore-based probes during offshore flow (see section 3.3 for the definition of onshore and offshore flow in this study). No strong correlation between background aerosol concentrations and wind speed was observed, with the exception of the timeframe of pure marine onshore flow (27–28 Nov 2006), when higher winds induced more sea spray production at the ocean, leading to an increase of the aerosol concentration as a function of wind speed. The concentration of submicron aerosols correlated well with humidity (correlation coefficient $cc \approx 0.65$ for 0.5 μm particles). This correlation reduced to 0.35 after humidity-induced growth effects were removed from the aerosol size distributions by normalization to RH = 80% using an algorithm given by *Fitzgerald* [1975], indicating that both onshore and offshore flow contained a considerable amount of hygroscopic submicron particles. This is expected for onshore flow, but not necessarily for offshore flow out of a semi-desert environment. In view of the diurnal sea-breeze cycle at Scripps, it is possible that the hygroscopic particles in the offshore flow are marine aerosols that had previously been moved inland by the sea-breeze.

4.2. Background Aerosols: FRF

[52] In contrast to Scripps, the FRF site is more exposed to the ocean and therefore wind speeds were much higher than at Scripps. Where the average wind speed during the Scripps experiment was only 0.9 m/s, with no wind speed higher than 9 m/s, the average wind speed at FRF was 4 m/s with maxima up to 20 m/s (see Table 2). Furthermore, the FRF site did not have a diurnal sea breeze and the airflow was determined by synoptic weather systems, resulting in longer cycles of onshore or offshore flow.

[53] The backward trajectory analysis showed that the air masses were pure maritime in origin in the beginning of the experiment, and became more and more of mixed marine-continental origin as the trial progressed. This was confirmed by a general increase of the Ångström coefficient (as measured with the handheld Sun photometer) over the course of the experiment. However, the Ångström coefficient varied considerably during a single day, taking values between 0.25 (pure marine) and 1.25 (strong continental influence). The cause of this variation is not known, but possible explanations are experimental errors, elevated aerosol layers passing over the site, or local (near-surface) airflow patterns.

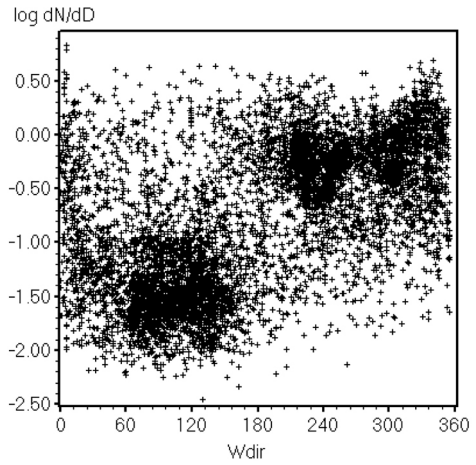

Figure 5. Log-concentrations of 5 μm particles as function of wind direction as measured at the shore-based station at Scripps.

[54] The concentrations as measured by probes 78 during onshore flow and by probes 57 during offshore flow (see Figure 3) provide information on the background aerosols advected to the site from elsewhere. The concentrations measured during onshore flow exhibit features typical of marine aerosols, i.e., strong correlation ($cc \approx 0.85$) with wind speed and wave energy dissipation. The correlation with humidity was weak for smaller particles, but reasonable ($cc \approx 0.5$) for larger particles. This correlation reduced to 0.3 after removing the humidity-induced growth effects. As expected, the aerosol concentrations measured during offshore flow did not correlate with wave energy dissipation. Correlation with wind speed was meager ($cc \approx 0.4$) and there was little evidence for humidity-induced growth, in accordance with a continental to continental-maritime nature.

4.3. Surf Aerosol Concentrations

[55] We now turn our attention to the aerosols generated over the surf zone, starting with the experiment at Scripps. Since the probes at Scripps remained in the same location during the whole experiment, the presence of surf-generated aerosols in the atmosphere can be demonstrated by a plot of aerosol concentration versus wind direction. Figure 5 shows the concentrations of particles of 5 μm diameter measured by the probe pair 46 at the shore-based station near Scripps pier. The plot includes all 7763 data points accumulated over the whole experiment. Figure 5 reveals that the aerosol concentration increased by 1–2 orders of magnitude when the flow changed from offshore (nominally 110°N) to onshore (290°N) and the aerosols generated over the surf zone could reach the probes. This corroborates well with the results reported by *de Leeuw et al.* [1997, 2000] for the same site.

[56] To further investigate the contribution of surf-generated aerosols, the differences $\delta(D)$ between the aerosol concentrations upwind and downwind of the surf zone were calculated by equation (4a). The calculations were made on a logarithmically spaced grid of 60 diameters ranging between 0.1 and 100 μm. A value of $\delta(D)$ was only calculated and entered if the diameter D was in the validity domains of the two polynomial fits to the measured distributions (see section 2.1). This process created size distributions of surf-generated aerosols, over a diameter range from 0.1–0.2 μm up to 8–15 μm (exact range varied from file to file). Four separate data sets were generated, for the 4 combinations of site and flow (e.g., onshore flow at Scripps). These data sets contained 1500–3000 data records each, as shown in Table 3. For FRF, the differences $\delta(D)$ were obtained from probes 46–57 and 46–78 (see Figure 3 for probe locations at FRF and Table 1 for probe numbers). Figure 3 shows that other combinations of probes would also yield difference concentrations providing information about surf aerosols (e.g., 78–5 or 78–23 for onshore flow). All these data sets were generated, but they turned out to be noisier, to result in smaller data sets, or to be less reliable because $\langle \Delta_{A\text{-}B}(D) \rangle$ (see section 2.1) was relatively large. Consequently, these data sets were not retained in the final analysis. As mentioned in section 2.5, probe 5 broke down near the end of the FRF experiment, which led to FRF offshore flow data set consisting of mixed 46–57 and 46–78 data. Although the probes should be interchangeable after the inter-comparison (see section 2.1), two secondary data sets with differences $\delta(D)$ were generated for FRF offshore flow: one consisting of 46–57 data and one of 46–78 data (see Table 3).

Table 3. Surf-Aerosol Data Sets[a]

Name	$\delta_{A\text{-}B}$	Number of Data Files	Symbol (Figure 6)
Onshore flow Scripps	23–46	2900	Solid triangle
Offshore flow Scripps	46–23	3250	Solid square
Onshore flow FRF	46–78	2750	Open triangle
Offshore flow FRF all events	46–57	1450	Open square
	46–78		
Offshore flow FRF event 1+2	46–57	800	Not shown
Offshore flow FRF event 3	46–78	650	Asterisk

[a]Column $\delta_{A\text{-}B}$ lists the aerosol probes used to create the difference (surf-aerosol) concentrations.

[57] Figure 6 shows the average size-resolved spectra of surf-generated aerosols for the various data sets. The Figure

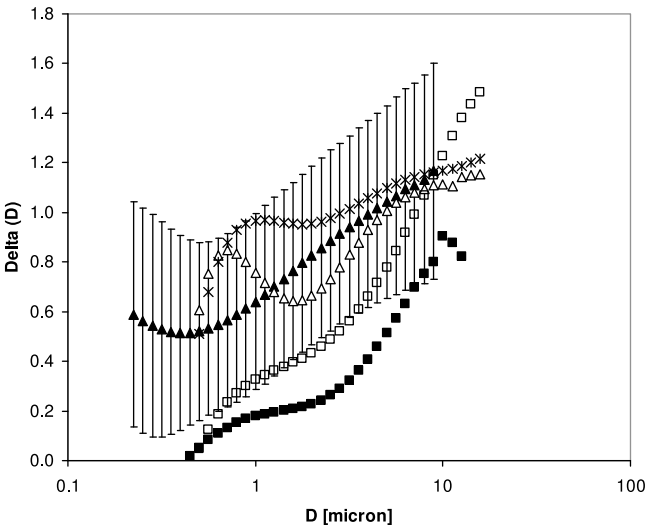

Figure 6. Size distributions of surf-generated aerosols in $\delta_{\log}(D)$ units (see text and equation 4b): solid triangles: onshore flow at Scripps, with standard deviations; solid squares: offshore flow at Scripps; open triangles: onshore flow at FRF; open squares: offshore flow at FRF; asterisks: 3rd offshore event at FRF.

Table 4. Regression Results for 5 μm Particles at Scripps[a]

	Data Set	Slope	cc	N	sdev	Δ(dN/dD)	$\Delta U/\Delta WED$
			Onshore				
Log dNdD versus U	Direct	0.033	0.153	2852	0.399	−1.5–0.5	0–9
Log dN/dD versus U	Difference	0.009	0.048	2624	0.366		
dN/dD versus *WED*	Direct	0.019	0.775	2831	0.304	−1.0–2.0	0–70
dN/dD versus *WED*	Difference	0.009	0.140	2812	0.686		
			Offshore				
Log dN/dD versus U	Direct	−0.207	−0.462	3221	0.435	−2.5–1.0	0–5.5
Log dN/dD versus U	Difference	−0.257	−0.515	2734	0.480		
dN/dD versus *WED*	Direct	0.021	0.967	3185	0.203	0.0–1.5	10–70
dN/dD versus *WED*	Difference	0.002	0.038	3033	0.489		

[a]The label *cc* denotes the correlation coefficient, N the number of data points includes in the regression, *sdev* the standard deviation of the fit, Δ(dN/dD) the dynamic range of the concentration (log-units), ΔU the dynamic range of wind speed, and ΔWED the dynamic range of wave energy dissipation. Labels "direct" and "difference" are explained in the text.

presents the factor $\delta_{\log}(D)$ (see section 3.2) by which the background concentration at a specific size has increased due to the surf contribution. Error bars are included for the data collected at Scripps during onshore flow. Standard deviations were comparable for other cases, but these have not been included for clarity. The scatter in the values of $\delta_{\log}(D)$ increased significantly for diameters larger than 10–15 μm, indicating that these parts of the spectra are less reliable. This is attributed to reduced probe sampling efficiency and a decreasing accuracy of the inter-comparison curves (see Figure 1). Because of the lesser reliability, the spectra were cut off at larger diameters. The data that was cut-off has not been included in the further analysis.

[58] The average spectra shown in Figure 6 correspond to different average meteorological conditions. Because of differences in average wind speed, wave height and wave energy dissipation, the source strength for surf-aerosol production must have been different, which implies that the absolute values cannot be compared. Instead, Figure 6 addresses the shape of the surf-aerosol spectrum. The curves with solid and open triangles and asterisks suggest that the surf zone adds approximately a factor of 3 to 5 particles at smaller (0.5 μm) diameters, increasing to a factor of 10 at larger (10 μm) diameters. This agrees reasonably well with the surf-aerosol spectra published by *Gathman and Smith* [1997] and *de Leeuw et al.* [2000] for Scripps. The relatively strong production at 5–10 μm coincides reasonably well with the peak diameter of jet-droplet production found for Oceanic source functions, and supports the views of *de Leeuw et al.* [2000], *Clarke et al.* [2006] and *O'Dowd and de Leeuw* [2007] that the surf aerosol source function resembles the Oceanic source function.

[59] On the other hand, two curves in Figure 6, with open and solid squares, suggest a much more pronounced increase in production for diameters approaching 10 μm, suggesting a peak beyond 10 μm. However, the uncertainty in our data at these larger diameters (see section 2.1) does not allow concluding firmly on the presence of this peak; all that can be said is that the production becomes relatively stronger at larger diameters. This pronounced production is found for two of the three data sets collected in offshore flow conditions. This might indicate that enhanced spume-droplet production played a role here as air and water move in opposite directions and droplets are more easily torn off the wave crests. However, further analysis led us to doubt this explanation. First, offshore winds at Scripps were very low, which does not favor spume droplet production, even by opposite motion of air and water. Second, the FRF offshore flow data measured by probe pair 46–78 only (curve with asterisks) does not at all suggest an enhanced production at larger diameters.

4.4. Regression Between Surf Aerosol Concentrations and Environmental Parameters

[60] As discussed in section 1, surf aerosol production has previously been parameterized in terms of wind speed (related to wave breaking and transport) and wave energy dissipation (*WED*, related to wave breaking on a sloping beach). Therefore, the regression analysis presented in this section focuses on these two parameters. Other environmental parameters (such as relative humidity and air-sea temperature difference) were less well correlated with the surf aerosol concentrations, or other parameters were closely related to one of the primary parameters (e.g., wave height was related to *WED*) and therefore not independent.

[61] The regression analysis was made for various diameters between 0.5 and 10 μm. Since there were no fundamental differences among the diameters, only the results for 5 μm particles will be discussed here. The data sets listed in Table 3 were input to the analysis. Since the complete FRF offshore flow data set and the one limited to probe data 46–57 gave almost identical results, the latter will not be further discussed here. The regression analysis was performed on the δ(D)-factors (see equation (4)) that represent the aerosol difference measurements (see section 2.1). Since the difference calculations inherently carry an uncertainty (even after inter-comparison), we looked for additional data sets to include in the regression analysis, in order to gain confidence in the results. Figure 6 suggests that the concentration of surf-generated aerosol particles of 5 μm was approximately 0.7 to 1 order of magnitude higher than the background concentrations, which implies that the majority of the particles sampled downwind of the surf zone can be attributed to surf-generated aerosols. Thus, there is justification in correlating these concentrations directly with meteorological and wave parameters and assuming that this reveals information about surf-generated aerosols.

[62] The results of the regression analysis (for 5 μm particles) are summarized in two tables: Table 4 presents the results for Scripps; Table 5 for FRF. The entries in the tables are labeled "direct" or "difference." The label "difference" refers to correlations with the δ(D)-factors, whereas "direct" refers to correlations with concentrations as measured by a single probe

Table 5. Regression Results for 5 μm Particles at FRF[a]

	Data Set	Slope	cc	N	Sdev	Δ(dN/dD)	$\Delta U/\Delta WED$
Onshore							
Log dN/dD versus *U*	Direct	0.067	0.800	1538	0.297	−2.0–0.5	0–20
Log dN/dD versus *U*	Difference	0.065	0.801	717	0.290		
dN/dD versus *WED*	Direct	0.012	0.936	1529	0.176	0.0–2.0	0–200
dN/dD versus *WED*	Difference	0.010	0.929	732	0.157		
Offshore							
Log dN/dD versus *U*	Direct	−0.018	−0.140	1028	0.304	−1.5–0.0	0–11
Log dN/dD versus *U*	Difference	−0.018	−0.272	727	0.141		
dN/dD versus *WED*	Direct	0.005	0.234	1023	0.164	0.0–1.0	10–50
dN/dD versus *WED*	Difference	0.005	0.022	727	0.143		
Offshore 3							
Log dN/dD versus *U*	Direct	−0.079	−0.649	504	0.243	−1.5–0.0	0–11
Log dN/dD versus *U*	Difference	−0.086	−0.654	246	0.261		
dN/dD versus *WED*	Direct	0.009	0.567	500	0.130	0.0–1.0	10–50
dN/dD versus *WED*	Difference	0.008	0.564	243	0.122		

[a]See Table 4 for an explanation of labels. The data set "offshore 3" corresponds to the 3rd offshore flow event at FRF, when probe pair 46–78 was deployed.

(e.g., probe 46 on the lower SIS-boom). The tables present the result of the regression analysis (slope, correlation coefficient, standard deviation of the fit and number of data points), as well as the dynamic range of the variables that were correlated. The tables show that the correlation between surf aerosol concentration and wave energy dissipation (*dN*/*dD* versus *WED*) is always positive, both for onshore and offshore flow. This then suggests a (linear) relation between surf aerosol production and wave energy dissipation.

[63] In contrast with this, the correlation between surf aerosol concentration and wind speed differs from onshore to offshore flow. For onshore flow, a positive slope is found, which could be indicative of a relation between surf aerosol production and wind speed as hypothesized by *de Leeuw et al.* [2000]. However, these authors only analyzed onshore flow cases and may not have noted the negative correlation between concentration and wind speed for offshore flow. This negative correlation is not consistent with a wind-driven production mechanism, and we thus conclude that wind speed is not the main driver for aerosol production. In our opinion, the negative correlation results from the opposing directions of wind and waves during offshore flow. In these conditions, stronger winds tend to suppress the wave heights and therefore WED. This hypothesis is supported by our data, which showed that the correlation between wind speed and *WED* was negative during offshore flow.

[64] In view of the results presented above, and especially the consistency between the sites and the flow direction, we conclude that WED is a better parameter than wind speed to describe surf aerosol production. The regression analysis presented above focused on a linear relation between *dN*/*dD* and *WED*. Since *Petelski and Chomka* [2000] used dimensional analysis to relate the surf aerosol flux to *WED* to the 3/4 power, we have also correlated *dN*/*dD* with $WED^{0.75}$. However, this did not significantly change the quality of the fits, and we can only conclude that the dependence of surf aerosol concentration on *WED* may be described by a function of the type WED^x, where *x* takes a value of approximately 1.

4.5. Vertical Concentration Gradients of Surf-Generated Aerosols

[65] As explained in section 3.5, vertical concentration gradients of the surf-generated aerosols are required to infer the surface flux of these aerosols. We did not measure aerosol gradients during our trial at Scripps pier, but information about the vertical profile of aerosols was collected during the experiment at FRF by the probes mounted in the lower and upper arms of the SIS (see Figure 3). Typically, the arms were positioned at 6 and 16.5 m above the sea surface, almost immediately downwind of the surf zone. For the 3 onshore events at FRF, we measured concentration gradients that were a factor of 2–5 larger than those measured by *de Leeuw et al.* [1997] at Scripps (parameterized by equation (11)). Furthermore, the observed gradients became steeper as wind speed increased, which does not corroborate with the assumption of more efficient vertical mixing with increasing winds as suggested by the few experimental measurements of aerosol vertical profiles available in the literature [*De Leeuw*, 1986; *Piazzola and Despiau*, 1997].

[66] To explain these findings, we turned to the experimental set-up at FRF. Due to the close proximity of the SIS to the surf zone, it was not a priori certain that surf-generated particles had time to disperse vertically to reach the upper probes. However, since probe 23 in the upper arm of the SIS (at 16.5 m above the surface; see Figure 3) typically measured 2–3 times more aerosols (for D = 5 μm) than probe 78 upwind of the surf (at 8.5 m above the surface), we conjecture that a fair amount of surf aerosols reached the upper probe, because the upwind probe only measures background aerosols. On the other hand, the aerosol concentration measured at the lower arm of the SIS increased more strongly with wave energy dissipation than that measured at the upper arm, resulting in stronger gradients at higher wind speeds. This indicates that there was not enough time for these surf-generated particles to disperse vertically to the upper arm of the SIS. Consequently, the concentration gradients as inferred from the PMS probes on the lower and upper arms of the SIS are overestimated. Since *de Leeuw et al.* [1997] measured the concentration gradients 50–100 m downwind of the surf zone there was more time for vertical mixing and their gradients should be more correct. Because these gradients corroborate well with theoretical and experimental evidence [*Gathman and Smith*, 1997; *van Eijk et al.*, 2001], we retained equation (11) as the gradient function for both the Scripps and FRF data. The vertical

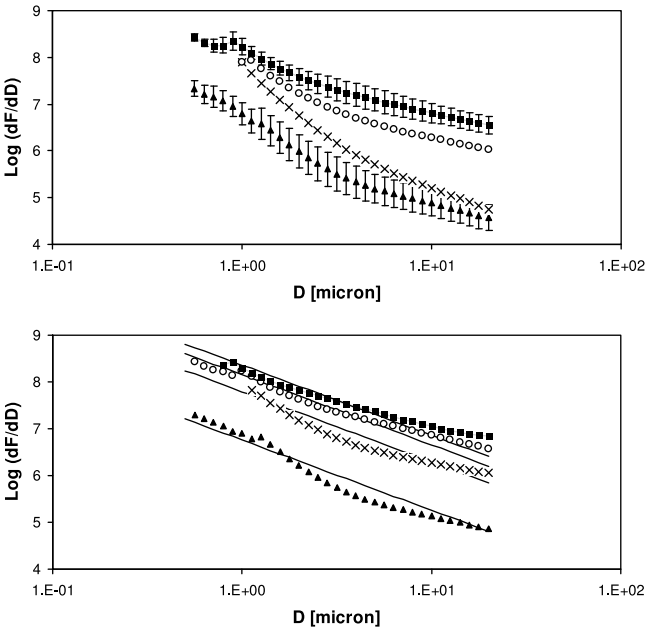

Figure 7. Surf aerosol fluxes dF/dD in [$\mu m^{-1}.m^{-2}.s^{-1}$] at diameter of formation. (top) Onshore flow at FRF; solid triangles: U = 0–5 m/s, with standard deviations; crosses: U = 5–10 m/s; open circles: U = 10–15 m/s; solid squares: U = 15–20 m/s, with standard deviations. (bottom) Onshore flow at FRF; solid triangles: *WED* = 0–50 W.m^{-2}; crosses: *WED* = 50–100 W.m^{-2}; open circles: *WED* = 100–150 W.m^{-2}; solid squares: *WED* = 150–200 W.m^{-2}. Lines denote approximations by equation (15).

profile measurements at FRF are now subject of a more extended analysis, which will be reported elsewhere.

4.6. Surf-Aerosol Fluxes

[67] The set of equations (5)–(11) allows calculating fluxes of surf-generated aerosols (see sections 3.4 and 3.5). As already mentioned, *de Leeuw et al.* [2000] used this same set of equations to analyze their data obtained at Scripps during onshore flow and to report a surf source function dF/dD in [$\mu m^{-1}.m^{-2}.s^{-1}$] in terms of wind speed and diameter:

$$\frac{dF}{dD} = k \cdot \exp(xU) \cdot D^y \qquad (14)$$

with $k = 1.1\ 10^7$, $x = 0.23$ and $y = -1.65$. It is assumed here that the factor of 10^7 is missing in the equation given by *de Leeuw et al.* [2000], although *Lewis and Schwartz* [2004] argue that the missing factor should be 10^6 rather than 10^7. The validity range of this equation was given as $0 < U < 9$ m/s and $0.5 < D < 20$ μm. When analyzing our own data for onshore flow at Scripps, we found $k = 4\ 10^7$, $x = 0.20$, and $y = -2.35$ for approximately the same ranges of U and D, which is relatively close in view of the uncertainties in the flux calculations.

[68] Equation (14) suggests an exponential increase of surf aerosol flux as function of wind speed. Contrary to the relatively low wind speeds at Scripps encountered by *de Leeuw et al.* [2000] and during our own trial at Scripps, the wind speeds at FRF during onshore flow conditions were considerably larger (see Table 2). This allowed us to study the wind speed dependence of dF/dD (as obtained by equation (8)) for higher winds, as shown in Figure 7 (top). The panel shows four spectra, each averaged over a 5 m/s wind speed interval. For clarity, standard deviations are only included for the smallest and largest winds; for the two other wind intervals similar uncertainties were found. The panel clearly shows that the increase of dF/dD with wind speed is less than exponential, and leads to the suggestion not to use equation (14) outside its validity regime $0 < U < 9$ m/s.

[69] However, the results of the present experiments at Scripps and FRF indicate that wave energy dissipation (*WED*) rather than wind speed is the driving environmental parameter for the generation of surf aerosols (see Tables 4 and 5). Therefore, the remainder of our analysis focused on *WED*. Figure 7 (bottom) shows the spectra of dF/dD at radius of formation averaged over four 50 W.m^{-2} intervals of *WED*. Standard deviations are not shown, but are comparable to those shown in Figure 7 (top). The spectra were obtained for onshore flow conditions at FRF, which offered the largest dynamic range in WED. At Scripps, and during offshore flow at FRF, the maximum values of WED were approximately 50–75 W.m^{-2}. Tables 4 and 5 show that the dependence of WED on concentration was fairly similar for all sites and flow conditions, which justifies focusing on FRF/onshore here. The Figure suggests then that dF/dD approaches a maximum for large values of *WED*. This is to be expected when the whitecap coverage over the surf zone reaches 100% (provided the length of the surf zone is constant). In that case, a further increase in *WED* does not produce more white water and thus there is no more increase in aerosol production. The data in Figure 7 (bottom) can be fitted to an equation for dF/dD as function of *WED*:

$$\left(\frac{dF}{dD}\right) = D^c \cdot 10^{\wedge}\left[\, a\left(1 - WED^b\right)\,\right] \qquad (15)$$

where $a = 10.0$, $b = -0.35$ and $c = -1.5$ and dF/dD is in [$\mu m^{-1}.m^{-2}.s^{-1}$]. The validity domain of equation (15) is $0.5 < D < 10$ μm and $10 < WED < 200$ W.m^{-2}. Figure 7 (bottom) includes 4 lines, calculated by equation (15) for WED-values of 25, 75, 125 and 175 W.m^{-2}, which allows estimating the quality of the fit to the data.

[70] Figure 8 puts equation (15) in perspective. The panel shows the surf-aerosol fluxes for the 30–50 W.m^{-2} *WED*-

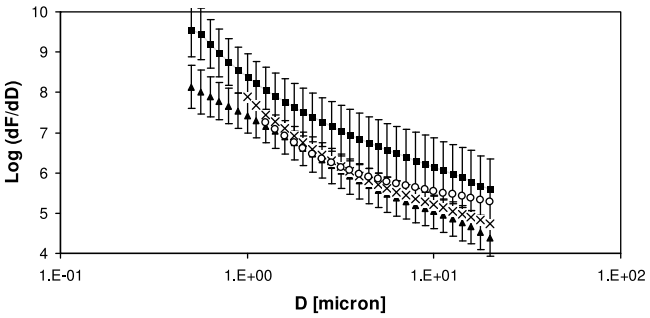

Figure 8. Surf aerosol fluxes dF/dD in [$\mu m^{-1}.m^{-2}.s^{-1}$] at diameter of formation for *WED* = 30–50 W.m^{-2}; crosses: FRF offshore flow; open circles: FRF onshore flow; solid triangles: Scripps offshore flow; solid squares: Scripps onshore flow. Standard deviations included for Scripps data.

interval for the four cases FRF-onshore, FRF-offshore, Scripps-onshore and Scripps-offshore. Standard deviations are included for the Scripps data only, but the error bars shown are also representative for the FRF-data. First, it is noted that the standard deviations are larger than in Figure 7; this is due to the smaller WED-interval, and hence, the smaller number of data points included in the average. The four curves demonstrate that there is an uncertainty in the absolute values of flux (governed by constant a in equation (15)) of about an order of magnitude, although one might decide to reject the quantitative results for Scripps obtained during offshore flow conditions because of non-ideal positioning of the aerosol probes (see section 2.4). On the other hand, the slopes of the four dF/dD versus D curves for Scripps and for FRF (governed by constant c in equation (15)) agree reasonably well within the experimental error. Additional plots (not shown here) demonstrated that the *WED*-dependence (constant b in equation (15)) is also rather similar for the four cases, albeit that the dynamic range of *WED* is limited to approximately 70 W.m^{-2} for all cases but FRF onshore. It is our opinion that a further discussion of the differences between the four curves in Figure 8 is not meaningful in view of the uncertainty in the flux calculations.

[71] Upon closer inspection, Figure 7 reveals that the slopes of the dF/dD versus D plot are not constant. The factor y of equation (14) seems to decrease with increasing U, whereas the factor c of equation (15) seems to decrease with increasing *WED*. When inspecting dF/dD versus D plots for *offshore* flow (not shown here), we found also a decrease of the slope with increasing U, but an increase of the slope with increasing *WED*. This different behavior of the slope as function of *WED* led us to believe that the variations in slope are governed by the variations in U. In our opinion, the changes in slope are an artifact resulting from the application of the gradient function, equation (11). As demonstrated in section 3.5, the fluxes of larger particles are strongly dependent on the choice of the gradient function. A slight imperfection in modeling the wind speed dependence in equation (11) may thus well be the cause for the variation of the slope of the dF/dD versus D plot with wind speed. On the other hand, one might also attribute the changes in slope to the formation of spume droplets: the higher the wind, the more (larger) droplets will be directly torn off the wave crests, in addition to the bubble-mediated production from breaking waves. However, this explanation is not confirmed by plots of the aerosol *concentrations* versus diameter (not shown here): if anything, the absolute values of the slopes of the dN/dD versus D plots tend to increase with wind speed.

4.7. Surf Aerosol Mass Fluxes

[72] Surf aerosol mass fluxes were calculated using equations (12) and (13) and an integration domain of 0.5–20 μm at diameter of formation (see section 3.6). Only those individual size distributions spanning the full integration domain were retained, and for these size distributions all difference concentrations $\delta(D)$ defined by equation (4) had to be positive. For the *WED*-interval 30–50 W.m^{-2}, and by including data from all 4 data sets (Scripps, FRF/onshore, offshore), this procedure yielded an average value of 50 ± 25 μg.m^{-2}.s^{-1} for the dry mass flux $F_{M,dry}$. This value dropped by approximately a factor of 5, when limiting the integration domain to 0.5–10 μm, which demonstrates that the contribution of the larger particles to the value of $F_{M,dry}$ is significant (see section 3.5). When applying the steeper gradient function in equation (10), by taking a constant of −0.1 instead of −0.075 in equation (11) (see section 3.5), the value of $F_{M,dry}$ (for the 0.5–20 μm integration domain) increased by 50%, which shows once more that small uncertainties in the concentrations and gradients of larger aerosol particles propagate strongly into the final flux calculations. The considerations above, and the understanding that the limited integration domain results in an underestimate of the mass flux, lead to the conclusion that the absolute value of $F_{M,dry}$ should be considered indicative at best.

[73] Nevertheless, it is instructive to compare F_M to values reported in literature. The present value of $F_{M,dry}$ = 50 μg.m^{-2}.s^{-1} corresponds to a wet mass flux of approximately 1500 μg.m^{-2}.s^{-1} (see section 3.6). Using instrumentation and models similar to ours, *de Leeuw et al.* [2000] reported wet mass fluxes between 297–858 μg.m^{-2}.s^{-1} for Moss Landing and between 562–1034 μg.m^{-2}.s^{-1} for Scripps pier, both times measured during onshore flow conditions. *de Leeuw et al.* [2000] integrated over a slightly smaller domain, i.e., 1.6–20 μm diameter at formation, as opposed to our domain of 0.5–20 μm. Our numerical tests (see above) suggest that this could have resulted in mass fluxes approximately 10% lower than ours. Furthermore, the values of *de Leeuw et al.* [2000] have not been averaged over a WED-interval of 30–50 W.m^{-2}, which makes a comparison more difficult. In view of this, we conclude that the mass fluxes as measured by *de Leeuw et al.* [2000] are of the same order of magnitude as the present results.

[74] *Chomka and Petelski* [1997] reported dry mass fluxes (M. Chomka, personal communication, 2010) between 3 and 384 μg.m^{-2}.s^{-1} for a site in Poland at the Baltic coast. Since these authors used impactors collecting efficiently particles of all sizes, one would expect that their technique provides a better estimate of the mass flux than our method that is based on an incomplete integration of the size distribution. On the other hand, the particles collected on the impactor microscopy glasses had to be counted by researchers using microscopes, which poses a severe risk for systematic errors. Furthermore, *Chomka and Petelski* [1997] made their measurements in waters that were highly oxygen super-saturated (132% O_2 saturation [*Marks*, 2008]). *Stramska et al.* [1990] have demonstrated that under those conditions the generation of jet and film droplets increases by a factor of 4 and 2.4, respectively. While the O_2 saturation values during our Scripps and FRF experiments have not been recorded, it is well possible that conditions were less extreme and hence, that jet and film droplet production was not as much enhanced. Taking all this into account, a quantitative comparison with *Chomka and Petelski* [1997] is difficult, although we note that our value $F_{M,dry}$ = 50 μg.m^{-2}.s^{-1} is of the same order of magnitude as those found by *Chomka and Petelski* [1997].

[75] *Petelski and Chomka* [2000] reported a linear relation between the dry mass flux $F_{M,dry}$ and $WED^{0.75}$ with slopes of 90.5 and 99.4 μg.m^{-2}.s^{-1} for various trials. For onshore flow conditions at FRF (the data set with the largest dynamic range of *WED*), we find a slope of 105 ± 2 μg.m^{-2}.s^{-1} with a correlation of 0.91 for the $F_{M,dry}$ versus $WED^{0.75}$ relation, which

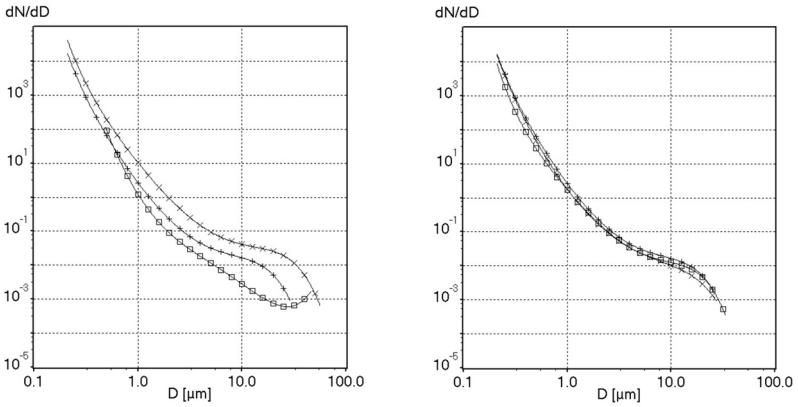

Figure 9. Transport experiment on 5 November. (left) Aerosol distributions dN/dD in [$\mu m^{-1}cm^{-3}$] near the surf zone; open squares: picnic table, probes 78; crosses: SIS, probes 46; pluses: Wahoo, probes 23. (right) Aerosol distributions measured at the Wahoo for 0.2 (pluses), 3 (crosses) and 12 km (open squares) from the pier.

is remarkably close to the values reported by *Petelski and Chomka* [2000]. However, the correlation between F_M versus $WED^{0.75}$ was less strong (or even absent) in our other data sets and the regression analysis (section 4.4) has shown that our data only allows concluding that the power factor for WED should be of the order of 1. Hence, we are hesitant to state that we have confirmed the 3/4 power law proposed by *Petelski and Chomka* [2000].

4.8. Horizontal Transport of Surf Aerosols Out to Sea

[76] During the FRF trial two transport experiments were performed to assess the advection of surf-generated aerosols out to sea (see section 2.6). Each experiment lasted about 4 h, during which time the conditions remained relatively constant. This was more true on 5 November ($\Delta WED < 3$ W.m^{-2}, $\Delta U < 2$ m/s, $\Delta RH < 10\%$, $\Delta ASTD < 1°$) than on 6 November ($\Delta WED < 5$ W.m^{-2}, $\Delta U < 4$ m/s, $\Delta RH < 15\%$, $\Delta ASTD < 2°$). However, on both days the reference concentrations at the picnic table and the lower boom of the SIS (measured by probes 78 and 46, respectively; see Figure 3) remained constant to within 0.3 log unit (or a factor 2 in absolute concentrations) during the 4 h timeframe. This implies that the surf source strength (as measured by the difference between the SIS and the picnic table) also remained constant to within a factor of 2.

[77] Figure 9 (left) shows the aerosol distributions as measured at the three stations at the start of the experiment on 5 November: picnic table (squares), lower boom of the SIS (crosses), and the Wahoo at 160 m distance from the pier (pluses). As expected, the offshore flow and the aerosol production in the surf zone result in a higher aerosol concentration downwind of the surf (SIS and Wahoo) than upwind of the surf (picnic table). This measurement also constitutes a baseline for the transport experiment: the SIS and the Wahoo should more or less measure the same aerosol concentration as both stations are located directly downwind of the surf zone. Our four baseline comparisons (start and end of experiment on 5 and 6 November) show that the differences between SIS and Wahoo never exceed 0.3 log unit –Figure 9 (left) shows the worst case. The differences between SIS and Wahoo may be due to the 3 m difference in height of the probes above the sea surface, to the spray water caused by the bow of the Wahoo that was turned into the wind, and to sampling of a different part of the surf zone.

[78] The aerosol distribution measured at the SIS constitutes a (continental) background and the surf contribution. When the air mass advects out over the sea, the concentration of these aerosols will decrease due to deposition. This decrease is countered by a build-up of locally generated marine sea-spray aerosols, but only to a certain extent, because the *onshore* flow measurements (see Figure 5) show that the surf zone has a stronger production than the Open Ocean. Figure 9 (right) shows the aerosol distribution as measured at the Wahoo at several distances downwind of the surf zone, up to 12 km, the maximum distance on 5 November. It is evident that there is no significant change in aerosol concentration over this distance. If anything, the decrease in concentration remained within the experimental error, of equivalently, the surf aerosol concentration has not decreased by more than a factor of two over 12 km. The experiments have been analyzed in more detail, by factoring in the time delay between measuring an air mass at the SIS and at the Wahoo downwind, and by specifically addressing surf-aerosol concentrations, but this did not change the conclusions reported above.

[79] The minimal decrease in concentration over 12 km is consistent with measurements by *Reid et al.* [2001], who have provided evidence for the formation of an internal boundary layer (IBL) under offshore flow conditions at FRF. Because the IBL confines the aerosol to a relatively shallow layer, a substantial concentration of marine aerosols (generated over water, not in the surf zone) could be built up. This build-up could have (partly) compensated the decrease of the concentration of surf-generated aerosols.

[80] For a better understanding of the net effect of deposition versus local sea-spray concentration build-up, we turned to numerical modeling. The MACMod numerical aerosol model [*Tedeschi and Piazzola*, 2010, 2011] was applied to assess the horizontal transport of the surf aerosols. This model is a two-dimensional unsteady model resolving the budget equation over a Cartesian grid (regular in the

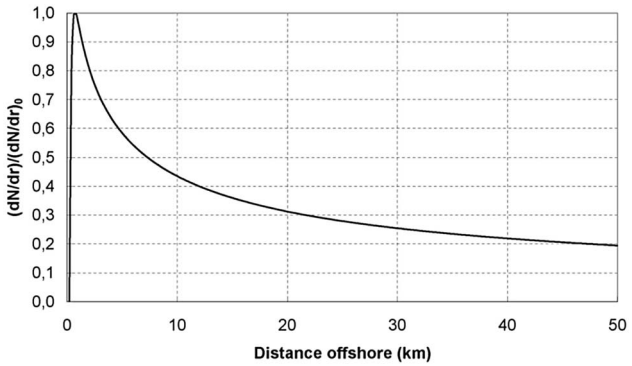

Figure 10. MACMod simulation of the relative aerosol concentration as function of distance downwind from the surf, for particles of 5 μm diameter at a height of 3 m.

horizontal direction and stretched in the vertical direction), using the finite volume method, *Patankar and Spalding* [1972]. An upwind scheme is used for the advection term and an implicit scheme is used for time integration. Turbulence closure is by the classical first-order eddy diffusion coefficient K, taking into account the atmospheric stability, the surface roughness, the particle inertia and the air rarefaction regime. Aerosol emission and removal at the sea surface is taken into account as an additional term for the vertical flux in the first layer. The model accepts two source functions at the bottom (horizontal) layer, i.e., a surf source function for the cell(s) corresponding to the surf zone, and an aerosol source function for oceanic conditions in the remainder of the domain.

[81] Figure 10 shows the results of the MACMod transport model, for particles of 5 μm diameter and for the meteorological conditions on 5 November (wind speed of 5 m/s). The panel presents the relative aerosol concentration as function of downwind distance, and demonstrates that the model predicts a decrease of the concentration of 5 μm particles by a factor of 2.5 at 12 km downwind. This decrease is only slightly more than the factor of 2 that represents the experimental error of our transport experiment (see above). In other words, the MACMod simulations may confirm the absence of a clear concentration decrease in our measurements. In hindsight, this suggests that the Wahoo should have sailed to appreciably larger downwind distances. However, this would have taken considerable time during which the offshore flow conditions would not have remained (relatively) stationary, thus resulting in a slowly decaying wavefield (and hence *WED* and surf aerosol production) over time.

[82] The results of the MACMod transport model are sensitive to the explicit models governing the various physical processes in play, which implies that caution is required when using the model for quantitative purposes. Nevertheless, the model results corroborate quite well with other modeling efforts reported in literature. Using the CAT model [*Vignati et al.*, 1998, 2001], *de Leeuw et al.* [2000] report a concentration decrease by a factor of 2–3 over 15 km for 10 μm particles in a 2 m/s wind. Using the same model, *Vignati et al.* [2001] report a concentration decrease by a factor of 2–10, depending on particle diameter, over 15 km and for an 8 m/s wind speed. In conclusion, the experimental and numerical efforts suggest that the effect of the surf zone pertains over several tens of kilometers out to sea.

5. Summary and Conclusions

[83] This paper reports on two experiments to establish the source strength of aerosols generated in the surf zone and their subsequent transport properties. The concentrations of the surf-generated particles over the diameter range 0.5–10 microns were inferred from difference measurements upwind and downwind of the surf zone. While this measurement principle seems straightforward, it turned out to be rather complicated. The complexity arises from the need to ensure an unobstructed airflow to the inlets of the probes, to allow proper sampling, and from the need for a careful intercalibration of the aerosol probes. Even so, we estimate that the difference concentrations reported here have an inherent uncertainty of several tenths of log-units, which amounts to concentration factors of up to 2–3.

[84] Our measurements clearly show that the surf zone adds 0.7–1 order of magnitude to the background aerosol concentration, arriving at the upwind side of the surf zone (see Figure 5). This confirms the ideas first brought forward by *Exton et al.* [1985] (followed by *Monahan* [1995]), and corroborates with earlier measurements by *Gathman and Smith* [1997], *de Leeuw et al.* [1997, 2000], *Hooper and Martin* [1999], and *Zielinski* [2003]. In accordance with *Gathman and Smith* [1997] and *de Leeuw et al.* [2000], we find that the spectrum of the surf-generated aerosols between 0.2 and 10 microns generally resembles the aerosol production functions for the open maritime environment. Our data did not permit reaching firm conclusions on differences in spectra between onshore and offshore flow (wind and waves in same or opposite directions), or between the Scripps and FRF sites (smooth sloped beach versus irregular beach).

[85] Regression analysis of the (surf) aerosol concentration, wind speed and wave energy dissipation shows that the latter parameter is better suited to describe the production of surf aerosols, as expected from a hydro-dynamical point of view of waves breaking on a sloped beach (see Tables 4 and 5). Other authors [*de Leeuw et al.*, 1997; *Neele et al.*, 1998] have hesitated to parametrize production in terms of wave energy dissipation, and finally settled for wind speed [*de Leeuw et al.*, 2000]. It is possible that this confusion has been caused by the strong correlation between wave energy dissipation and wind speed, the restriction of only considering onshore flow, and the limited dynamic range of environmental parameters encountered during their trials. Our data shows that the aerosol concentration is always positively correlated with wave energy dissipation, but that in offshore flow conditions anti-correlation may exist with wind speed. Furthermore, appreciable dynamic ranges of the most important variables (wave energy dissipation, wind speed) are required to clearly establish the relations with aerosol concentration. In this respect, our measurements at FRF proved instrumental.

[86] By application of a box transport model and the continuity equation (see equations (8)–(11)), the difference aerosol concentrations have been converted into aerosol fluxes. It turns out that the uncertainty in the values of the difference concentrations propagates strongly into the flux

values. In addition, the conversion requires a function describing the vertical concentration gradients of the surf-generated aerosols. Not only is this function difficult to establish experimentally, the flux values are also very sensitive to the exact gradient function used, especially for larger diameters (see Figure 4). Consequently, we estimate that there is an appreciable uncertainty in the absolute values of the aerosol fluxes. Nevertheless, the flux of surf-generated aerosols can be expressed in terms of wave energy dissipation (WED), resulting in a source function dF/dD in [$\mu m^{-1}.m^{-2}.s^{-1}$] for surf-generated aerosols, at radius of formation:

$$\left(\frac{dF}{dD}\right) = D^c \cdot 10^{\wedge}\left[\, a\left(1 - WED^b\right)\,\right] \tag{16}$$

where $a = 10.0$, $b = -0.35$ and $c = -1.5$. The validity domain of equation (16) is $0.5 < D < 10$ μm and $10 < WED < 200$ W.m^{-2}. We consider equation (16) an approximate source function, which does not attempt to explain differences between onshore and offshore flow, nor between the two experimental sites, Scripps and FRF. While we caution the reader regarding the uncertainty in the coefficient a of equation (16), we feel more confident about the WED-dependence and the power factor c.

[87] Since the evaluation of *WED* requires knowledge of the incoming wavefield and the bathymetry profile of the surf zone [cf. *Francius et al.*, 2007], those using equation (16) may wish to retrieve an approximate value for *WED* from the average wave height, H_{rms}. Based on regression analysis between *WED* in [W.m^{-2}] and H_{rms} in [m] at FRF and Scripps, we suggest the approximate relation, for $0.1 < H_{rms} < 5$m:

$$WED = -3 + 35 \cdot H_{rms}. \tag{17}$$

[88] For onshore flow conditions at Scripps, *de Leeuw et al.* [2000] presented a source function for surf-generated aerosols based on wind speed (see equation (14) of the present paper). Our own measurements confirm their results, but only for onshore flow and only for the low to medium wind speeds ($U < 9$ m/s). Although the source function given by *de Leeuw et al.* [2000] may be easier to use than our source function based on WED, we consider our WED-based source function to be more general.

[89] When the aerosol flux values are integrated over the size distribution, the total mass flux F_M is obtained. For the WED-interval between 30 and 50 W.m^{-2}, the average dry mass flux over all data (Scripps, FRF/onshore, offshore) was $F_{M,dry} = 50 \pm 25$ μg.m^{-2}.s^{-1}. The large standard deviation shows that all uncertainties in difference concentration and flux calculations propagate strongly into the values of F_M. In view of this large uncertainty, our findings for F_M corroborate well with values reported previously by *de Leeuw et al.* [2000]. In addition, limitations in our data collection instruments prevent us from completing the integral over the full size distribution of surf-generated aerosols, resulting in an underestimation of F_M by as much of a factor of 5., Taking this into account, our values are of the same order as those reported by *Chomka and Petelski* [1997] using an impactor technique. The latter authors used dimensional analysis to infer a 3/4 power dependence between F_M and wave energy dissipation (*WED*). Our data obtained at FRF during onshore flow conditions (which have the largest dynamic range of WED), support this relation, but the uncertainty is such that the 3/4 power dependence cannot be ascertained beyond doubt: our results are consistent with a power law and an exponent of the order of 1.

[90] During (relatively) stable offshore flow conditions at FRF, we attempted two transport experiments to assess the typical distance to which the surf-generated aerosols are advected out to sea. At maximum range (12–16 km), there was still no noticeable decrease of the aerosol concentration (i.e., not more than a factor of 2) as compared to the reference concentration measured directly downwind of the surf zone (see Figure 9). This suggests that the surf-generated particles are transported over appreciable distances, in accordance with observations [*Kunz et al.*, 2002; *Zielinski*, 2003], previous modeling efforts [*de Leeuw et al.*, 2000; *Vignati et al.*, 1998] and our own modeling efforts with the MACMod model [*Tedeschi and Piazzola*, 2011].

[91] In conclusion, our experiments have provided new elements for the understanding of the generation and behavior of sea-spray aerosols over the surf zone. Although much effort was made to identify the error sources in the measurements and subsequent analyses, uncertainties remain, especially in quantitative results. Therefore, further research on this topic is encouraged.

[92] **Acknowledgments.** We acknowledge our technicians Marcel Moerman, Leo Cohen, Peter Frits and Tathy Missamou for their instrumental help during the experiments. We also acknowledge Eric Terrill and the staff of the Scripps Institution of Oceanography (SIO), for making available Scripps pier and valuable assistance in the experiment. Robert Frouin of SIO moved the NASA Aeronet Sun photometer from its normal location to the end of Scripps pier. Dimitri Tsintikidis and his staff at the SPAWAR System Center, San Diego, CA, provided essential assistance in receipt, moving and setting up the instruments sent over from TNO in the Netherlands. They also provided a Sun photometer during both experiments. Bill Birkemeier and Brian Scarborough of the U.S. Army Corps of Engineers Field Research Facility (FRF) in Duck NC made it possible for us to use the FRF pier for our second experiment and provided essential assistance during the experiment. Gerrit de Leeuw of the University of Helsinki, Finland, loaned two aerosol scattering spectrometers (probes 5 and 8), and Droplet Technologies Inc loaned us the fog monitor (probe 7). Finally, we acknowledge the financial support of the USA Department of Defense under contract FA9451-06-D-0008/0001 and we thank the anonymous reviewers of the manuscript for their many valuable remarks.

References

Andreae, M. O. (1995), Climate effects of changing atmospheric aerosol levels, in *World Survey of Climatology*, vol. 16, *Future Climate of the World*, edited by A. Henderson-Sellers, pp. 341–392, Elsevier, New York.

Andreas, E. L. (1992), Sea spray and the turbulent air-sea fluxes, *J. Geophys. Res.*, *97*, 11,429–11,441, doi:10.1029/92JC00876.

Andreas, E. L. (1998), A new sea spray generation function for wind speeds up to 32 m/s, *J. Phys. Oceanogr.*, *28*, 2175–2184, doi:10.1175/1520-0485(1998)028<2175:ANSSGF>2.0.CO;2.

Andreas, E. L. (2002), A review of the sea spray generation function for the open ocean, in *Atmosphere-Ocean Interactions*, vol. 1, edited by W. A. Perrie, pp. 1–46, WIT Press, Southampton, U. K.

Ångström, A. (1929), On the atmospheric transmission of sun radiation and on dust in the air, *Geogr. Ann.*, *11*, 156–166, doi:10.2307/519399.

Baldock, T. E., P. Holmes, S. Bunker, and P. van Weert (1998), Cross-shore hydro-dynamics within an unsaturated surf zone, *Coastal Eng.*, *34*, 173–196, doi:10.1016/S0378-3839(98)00017-9.

Battjes, J. A., and J. P. Janssen (1978), Energy loss and setup due to breaking of random waves, paper presented at 16th International Conference on Coastal Engineering, ASCE, New York.

Blanchard, D. C. (1963), The electrification of the atmosphere by particles from bubbles in the sea, *Prog. Oceanogr.*, *1*, 73–112, doi:10.1016/0079-6611(63)90004-1.

Blanchard, D. C. (1966), Positive space charges from the sea, *J. Atmos. Sci.*, *23*, 507–515, doi:10.1175/1520-0469(1966)023<0507:PSCFTS>2.0.CO;2.

Blanchard, D. C., and A. H. Woodcock (1957), Bubble formation and modifications in the sea and its meteorological significance, *Tellus*, *9*, 145–158, doi:10.1111/j.2153-3490.1957.tb01867.x.

Blot, R. (2009), Etude et modélisation de la variation spatio-temporelle des concentrations d'aérosols en zone côtière, Ph.D. thesis, Univ. du Sud de Toulon-Var, Sud de Toulon-Var, France.

Charlson, R. J., S. E. Schwartz, J. M. Hales, R. D. Cess, J. A. Coakley Jr., J. E. Hansen, and D. J. Hoffman (1992), Climate forcing by anthropogenic aerosols, *Science*, *255*, 423–430, doi:10.1126/science.255.5043.423.

Chomka, M., and T. Petelski (1997), Modeling of the sea aerosol emission by the coastal zone, *Oceanologia*, *39*, 211–225.

Clarke, A. D., S. R. Owens, and J. Zhou (2006), An ultrafine sea-salt flux from breaking waves: Implications for cloud condensation nuclei in the remote marine atmosphere, *J. Geophys. Res.*, *111*, D06202, doi:10.1029/2005JD006565.

de Jong, A. N., A. M. J. van Eijk, P. J. Fritz, L. H. Cohen, and M. M. Moerman (2007), The use of multi-band transmission data, collected at Scripps pier in November 2006, for the investigation of aerosol characteristics, *Proc. SPIE Int. Soc. Opt. Eng.*, *6708*, 67080L, doi:10.1117/12.730479.

de Leeuw, G. (1986), Vertical profiles of giant particles close above the sea surface, *Tellus, Ser. B*, *38*, 51–61, doi:10.1111/j.1600-0889.1986.tb00087.x.

de Leeuw, G. (1993), Aerosols near the air-sea interface, *Trends Geophys. Res.*, *2*, 55–70.

de Leeuw, G., F. P. Neele, A. M. J. van Eijk, E. Vignati, M. Hill, and M. H. Smith (1997), Aerosol production in the surf zone and effects on IR extinction, *Proc. SPIE Int. Soc. Opt. Eng.*, *3125*, 14 pp.

de Leeuw, G., F. P. Neele, M. Hill, M. H. Smith, and E. Vignati (2000), Production of sea spray in the surf zone, *J. Geophys. Res.*, *105*, 29,397–29,409, doi:10.1029/2000JD900549.

Dubovik, O., and M. D. King (2000), A flexible inversion algorithm for retrieval of aerosol optical properties from Sun and sky radiance measurements, *J. Geophys. Res.*, *105*, 20,673–20,696, doi:10.1029/2000JD900282.

Exton, H. J., J. Lathma, P. M. Park, S. J. Perry, M. H. Smith, and R. R. Allan (1985), The production and dispersal of marine aerosol, *Q. J. R. Meteorol. Soc.*, *111*, 817–837, doi:10.1256/smsqj.46908.

Fitzgerald, J. W. (1975), Approximation formulas for the equilibrium size of an aerosol particle as a function of its dry size and composition and the ambient relative humidity, *J. Appl. Meteorol.*, *14*, 1044–1049, doi:10.1175/1520-0450(1975)014<1044:AFFTES>2.0.CO;2.

Francius, M. J., J. Piazzola, P. Forget, O. Le Calve, and J. T. Kusmierczyk-Michulec (2007), Sea spray aerosol and wave energy dissipation in the surf zone, *Proc. SPIE Int. Soc. Opt. Eng.*, *6708*, 67080N, doi:10.1117/12.734261.

Gathman, S. G. (1983), Atmospheric electric space charge near the ocean surface, in *Oceanic Whitecaps*, edited by E. C. Monahan and G. Mac Nicaill, pp. 227–243, D. Reidel, New York.

Gathman, S. G., and W. A. Hoppel (1970), Surf electrification, *J. Geophys. Res.*, *75*, 4525–4529, doi:10.1029/JC075i024p04525.

Gathman, S. G., and M. H. Smith (1997), On the nature of surf-generated aerosol and their effect on electro-optical systems, *Proc. SPIE Int. Soc. Opt. Eng.*, *3125*, 2–12, doi:10.1117/12.283882.

Holben, B. N., D. Tanre, and A. Smirnov (2001), An emerging ground-based aerosol climatology: Aerosol optical depth from AERONET, *J. Geophys. Res.*, *106*, 12,067–12,097, doi:10.1029/2001JD900014.

Hooper, W. P., and L. U. Martin (1999), Scanning lidar measurements of surf-zone aerosol generation, *Opt. Eng.*, *38*, 250–255, doi:10.1117/1.602083.

Intergovernmental Panel on Climate Change (IPCC) (2008), *Climate Change 2007: The Physical Science Basis. Contribution of Working Group I to the Fourth Assessment Report of the Intergovernmental Panel on Climate Change*, Cambridge, Univ. Press, Cambridge, U. K.

Jaenicke, R. (1984), Physical aspects of atmospheric aerosol, in *Aerosols and Their Climatic Effects*, edited by H. E. Gerbard, pp. 7–34, A. Deepak, Hampton, Va.

Jensen, D. R., C. R. Zeisse, K. M. Littfin, and S. G. Gathman (1997), EOPACE (Electro-Optical Propagation Assessment in Coastal Environments) overview and initial accomplishments, *Proc. SPIE Int. Soc. Opt. Eng.*, *3125*, 98–108, doi:10.1117/12.279017.

Kunz, G. J., G. de Leeuw, E. Becker, and C. D. O'Dowd (2002), Lidar observations of atmospheric boundary layer structure and sea spray aerosol plumes generation and transport at Mace Head, Ireland (PARFORCE experiment), *J. Geophys. Res.*, *107*(D19), 8106, doi:10.1029/2001JD001240.

Kusmierczyk-Michulec, J. T., and A. M. J. van Eijk (2007), The Ångström coefficient as a tracer of the continental aerosols, *Proc. SPIE Int. Soc. Opt. Eng.*, *6708*, 67080P, doi:10.1117/12.732426.

Kusmierczyk-Michulec, J. T., A. M. J. van Eijk, M. M. Moerman, L. H. Cohen, A. N. de Jong, and P. J. Fritz (2008), Transmissometer versus Sun photometer measurements of the aerosol optical properties, *Proc. SPIE Int. Soc. Opt. Eng.*, *7090*, 70900L, doi:10.1117/12.797837.

Laskin, A., D. J. Gaspar, W. Wang, S. W. Hunt, J. P. Cowin, S. D. Colson, and B. J. Finlayson-Pitts (2003), Reactions at interfaces as a source of sulfate formation in sea-salt particles, *Science*, *301*, 340–344, doi:10.1126/science.1085374.

Lewis, E. R., and S. E. Schwartz (Eds.) (2004), *Sea Salt Aerosol Production: Mechanisms, Methods, Measurements and Models: A Critical Review*, *Geophysical Monogr. Ser.*, vol. 152, 413 pp., AGU, Washington, D. C.

Longuet-Higgins, M. S., and R. W. Stewart (1963), A note on wave set-up, *J. Mar. Res.*, *21*, 4–10.

Mallet, M., J. C. Roger, S. Despiau, O. Dubovik, and J. P. Putaud (2003), Microphysical and optical properties of aerosol particles in urban zone during ESCOMPTE, *Atmos. Res.*, *69*, 73–97, doi:10.1016/j.atmosres.2003.07.001.

Marks, R. (2008), Dissolved oxygen supersaturation and bubble formation in the southern Baltic Sea coastal waters, *Hydrol. Res.*, *39*, 229–236, doi:10.2166/nh.2008.021.

Monahan, E. C. (1995), *Coastal Aerosol Workshop Proceedings*, edited by A. K. Goroch and G. L. Geernaert, *Rep. NRL/MR/7542–95–7219*, Naval Res. Lab., Monterey, Calif.

Monahan, E. C., D. E. Spiel, and K. L. Davidson (1986), A model of marine aerosol generation via whitecaps and wave disruption, in *Oceanic Whitecaps*, edited by E. C. Monahan and G. McNiocaill, pp. 167–174, D. Reidel, Norwell, Mass.

Mulcahy, J. P., C. D. O'Dowd, S. G. Jennings, and D. Ceburnis (2008), Significant enhancement of aerosol optical depth in marine air under high wind conditions, *Geophys. Res. Lett.*, *35*, L16810, doi:10.1029/2008GL034303.

Neele, F. P., G. de Leeuw, M. Jansen, and M. Stive (1998), Quantitative assessment of surf-produced sea spray aerosol, *Proc. SPIE Int. Soc. Opt. Eng.*, *3433*, 53, doi:10.1117/12.330242.

O'Dowd, C. D., and G. de Leeuw (2007), Marine aerosol production: A review of the current knowledge, *Philos. Trans. R. Soc. A*, *365*, 1753–1774, doi:10.1098/rsta.2007.2043.

Patankar, S. V., and D. B. Spalding (1972), A calculation procedure for heat, mass and momentum transfer in three-dimensional parabolic flows, *Int. J. Heat Mass Transfer*, *15*, 1787–1806, doi:10.1016/0017-9310(72)90054-3.

Petelski, T., and M. Chomka (1996), Marine aerosol fluxes in the coastal seas–BAEX experimental data, *Oceanologia*, *38*, 469–484.

Petelski, T., and M. Chomka (2000), Sea salt emission from the coastal zone, *Oceanologia*, *42*, 399–410.

Piazzola, J. G. T., and R. Blot (2010), Spatial variation of the aerosol concentration and deposition over the Mediterranean coastal zone, *Atmos. Res.*, *97*, 214–228, doi:10.1016/j.atmosres.2010.04.003.

Piazzola, J., and S. Despiau (1997), Vertical distribution of aerosol particles near the air-sea interface in coastal zone, *J. Aerosol Sci.*, *28*, 1579–1599, doi:10.1016/S0021-8502(97)00020-7.

Piazzola, J., and S. Despiau (2002), A sea spray generation function for fetch-limited conditions, *Ann. Geophys.*, *20*, 121–131, doi:10.5194/angeo-20-121-2002.

Piazzola, J., P. Forget, C. Lafon, and S. Despiau (2009a), Spatial variation of sea-spray fluxes over a Mediterranean coastal zone using a sea state model, *Boundary Layer Meteorol.*, *132*, 167–183, doi:10.1007/s10546-009-9386-2.

Piazzola, J., G. Tedeschi, and M. Francius (2009b), Contributions to the JDF&A surf aerosol project, edited by A. M. J. van Eijk, *Rep. TNO-DV 2009 C233*, TNO Defense, Security and Safety, The Hague, Netherlands.

Pickering, K. E., et al. (2001), Trace gas transport and scavenging in PEM-Tropics B South Pacific Convergence Zone convection, *J. Geophys. Res.*, *106*, 32,591–32,602, doi:10.1029/2001JD000328.

Porter, J. N., B. R. Lienert, S. K. Sharma, E. Lau, and K. Horton (2003), Vertical and horizontal aerosol scattering fields over Bellows Beach, Oahu, during the SEAS experiment, *J. Atmos. Oceanic Technol.*, *20*, 1375–1387, doi:10.1175/1520-0426(2003)020<1375:VAHASF>2.0.CO;2.

Reid, J. S., H. H. Jonsson, M. H. Smith, and A. Smirnov (2001), Evolution of the vertical profile and flux of large sea-salt particles in a coastal zone, *J. Geophys. Res.*, *106*, 12,039–12,053, doi:10.1029/2000JD900848.

Reid, J. S., B. Brooks, K. K. Crahen, D. A. Hegg, T. F. Eck, N. O'Neill, G. de Leeuw, E. A. Reid, and K. D. Anderson (2006), Reconciliation of coarse mode sea-salt aerosol particle size measurements and parameterizations at a subtropical ocean receptor site, *J. Geophys. Res.*, *111*, D02202, doi:10.1029/2005JD006200.

Schoeberl, M. R., and P. A. Newman (1995), A multiple-level trajectory analysis of vortex filaments, *J. Geophys. Res.*, *100*, 25,801–25,815, doi:10.1029/95JD02414.

Shi, J., D. L. Zhao, X. Q. Li, and Z. Zhong (2009), New wave-dependent formulae for sea-spray flux at air-sea interface, *J. Hydrodyn., Ser. B*, *21*, 573–581, doi:10.1016/S1001-6058(08)60186-9.

Sievering, H., J. Cainey, M. Harvey, J. McGregor, S. Nichol, and A. P. Quinn (2004), Aerosol non-sea-salt sulphate in the remote marine boundary layer under clear-sky and normal cloudiness conditions: Ocean-derived biogenic alkalinity enhances sea-salt sulphate production by ozone oxidation, *J. Geophys. Res.*, *109*, D19317, doi:10.1029/2003JD004315.

Smirnov, A., B. N. Holben, T. F. Eck, O. Dubovik, and I. Slutsker (2000), Cloud screening and quality control algorithms for the AERONET data base, *Remote Sens. Environ.*, *73*, 337–349, doi:10.1016/S0034-4257(00)00109-7.

Smith, M. H., P. M. Park, and I. E. Consterdine (1993), Marine aerosol concentrations and estimated fluxes over the sea, *Q. J. R. Meteorol. Soc.*, *119*, 809–824, doi:10.1002/qj.49711951211.

Spiel, D. E. (1994), The sizes of jet drops produced by air bubbles bursting on sea- and fresh-water surfaces, *Tellus, Ser. B*, *46*, 325–338.

Spiel, D. E. (1997), A hypothesis concerning the peak in film drop production as a function of bubble size, *J. Geophys. Res.*, *102*, 1153–1161, doi:10.1029/96JC03069.

Stramska, M., R. Marks, and E. C. Monahan (1990), Bubble-mediated aerosol production as a consequence of wave breaking in supersaturated (hyperoxic) seawater, *J. Geophys. Res.*, *95*, 18,281–18,288, doi:10.1029/JC095iC10p18281.

Tedeschi, G., and J. Piazzola (2010), Study of vertical transport of marine aerosol using an unsteady 2D model, paper presented at 31st NATO/SPS International Technical Meeting on Air Pollution Modeling and its Application, NATO, Torino, Italy.

Tedeschi, G., and J. Piazzola (2011), Development of a 2D marine aerosol transport model, application to the influence of thermal stability in the marine atmospheric boundary layer, *Atmos. Res.*, *101*, 469–479, doi:10.1016/j.atmosres.2011.04.013.

Terray, E. A., M. A. Donelan, Y. C. Agrawal, W. M. Drennan, K. K. Kahma, A. J. Williams III, P. A. Hwang, and S. A. Kitaigorodskii (1996), Estimates of the kinetic energy dissipated under breaking waves, *J. Phys. Oceanogr.*, *26*, 792–807, doi:10.1175/1520-0485(1996)026<0792:EOKEDU>2.0.CO;2.

Thornton, E. B., and R. T. Guza (1986), Surf zone longshore currents and random waves: Field data and models, *J. Phys. Oceanogr.*, *16*, 1165–1178, doi:10.1175/1520-0485(1986)016<1165:SZLCAR>2.0.CO;2.

van Eijk, A. M. J., and G. de Leeuw (1992), Modeling aerosol particle size distributions over the North Sea, *J. Geophys. Res.*, *97*, 14,417–14,429, doi:10.1029/92JC01214.

van Eijk, A. M. J., B. J. S. Tranchant, and P. G. Mestayer (2001), SeaCluse: Numerical simulation of evaporating sea spray droplets, *J. Geophys. Res.*, *106*, 2573–2588, doi:10.1029/2000JC000377.

van Eijk, A. M. J., J. T. Kusmierczyk-Michulec, and D. L. Merritt (2009), Surf aerosols, *Rep. TNO-DV 2009 C232*, TNO Defense, Security and Safety, The Hague, Netherlands.

Vignati, E., G. de Leeuw, and R. Berkowicz (1998), Aerosol transport in the coastal environment and effects on extinction, *Proc. SPIE Int. Soc. Opt. Eng.*, *3433*, 21, doi:10.1117/12.330223.

Vignati, E., G. de Leeuw, and R. Berkowicz (2001), Modeling coastal aerosol transport and effects of surf-produced aerosols on processes in the marine atmospheric boundary layer, *J. Geophys. Res.*, *106*, 20,225–20,238, doi:10.1029/2000JD000025.

Woolf, D. K. (1997), Bubbles and their role in gas exchange, in *The Sea Surface and Global Change*, edited by P. S. Liss and R. A. Duce, pp. 173–206, Cambridge Univ. Press, Cambridge, U. K., doi:10.1017/CBO9780511525025.007.

Zielinski, T. (2003), Dependence of the surf zone aerosol on wind direction and wind speed at a coastal site on the Baltic Sea, *Oceanologia*, *45*, 359–371.

M. J. Francius, J. Piazzola, and G. Tedeschi, Laboratoire de Sondages Electromagnétiques de l'Environnement Terrestre, UMR 6017 CNRS, Université du Sud Toulon-Var, BP 56, F-83162 La Valette du Var, France.

J. T. Kusmierczyk-Michulec, Institute of Oceanology, Polish Academy of Sciences, PO Box 148, 81-712 Sopot, Poland.

D. L. Merritt and J. D. Fontana, JDF&A Inc., 17095 Obsidian Dr., Ramona, CA 92065, USA.

A. M. J. van Eijk, TNO, PO Box 96864, NL-2509 JG The Hague, Netherlands. (lex.vaneijk@tno.nl)